Navneet_OPP

by Prabal Pratap Singh Bhadauria

Submission date: 14-Jun-2025 05:56AM (UTC+0530)
Submission ID: 2696574153
File name: Navneet_OPP.pdf (577.93K)
Word count: 27941
Character count: 157985

Abstract

The rapid expansion of the agricultural sector has led to a significant increase in agricultural waste. Crop residues such as corn, rice, sugarcane, and wheat are often openly burned, despite the detrimental environmental consequences. In addition to agricultural waste, a substantial portion of the food produced is also wasted and left to decompose without proper disposal mechanisms. From both environmental and energy perspectives, the most effective waste management strategy involves utilizing these wastes to synthesize value-added products. Rice husk ash (RHA) and eggshells (ES) are among the most abundant agro-food wastes and represent promising sources of SiO_2 and $CaCO_3$, respectively. These agro-food wastes or ashes are consist of various trace elements such as silica, calcium, and magnesium typically required for the production of bioglass and bioglass-ceramics. Furthermore, agro-food wastes offer sustainable and environmentally friendly alternatives to conventional precursors. This study focuses on the synthesis of hybrid glasses with a base composition of $43SiO_2$-25CaO-$25Na_2O$-$7P_2O_5$ (wt%) using biowaste-derived silica and calcium, supplemented with conventional precursors. The effects of systematically substituting CaO with MgO and Na_2O with K_2O were investigated. The resulting glasses and glass-ceramics were characterized to determine their physical, structural, thermal, and mechanical properties to assess their suitability as biomaterials. The *in-vitro* bioactive properties were evaluated *in-vitro* using simulated body fluid (SBF). Furthermore, biocompatibility was assessed using the 3-(4,5-dimethylthiazol-2-yl)-2,5-diphenyltetrazolium bromide (MTT) assay in human peripheral blood mononuclear cells (PBMC). This thesis is organized into five chapters.

Chapter 1 provides a basic understanding of biomaterials, with a specific focus on bioglasses and glass-ceramics, and the essential requirements for these materials to be considered bioactive. It outlines various testing methods

employed to assess the bioactivity of glasses and glass-ceramics, including a detailed explanation of the hydroxyapatite (HAp) layer formation mechanism on the material surface upon immersion in SBF. The biocompatibility testing methods are also given in brief. The 3-(4,5-dimethylthiazol-2-yl)-2,5-diphenyl tetrazolium bromide (MTT) assay to assess the biocompatibility of glass and glass-ceramic materials is also discussed. The reliability of this method stems from its direct correlation with viable cell counts. Additionally, the chapter explores the potential of agro-food waste and its components.

Chapter 2 presents a comprehensive review of the existing literature on sustainable bioactive glasses, with a particular emphasis on the utilization of agro-food waste as a precursor source. The review explores the potential of various agro-food wastes, including RHA and ESP, as sustainable alternatives to conventional materials in bioactive glass synthesis. Different processing techniques for extracting valuable minerals from these waste sources are examined, along with a discussion of various synthesis methods employed for producing bioactive glasses and glass-ceramics. The review analyzes the crucial structure-property relationships in these materials, highlighting the influence of composition and processing parameters on bioactivity, biocompatibility, and mechanical properties. Furthermore, the *in-vitro* and *in-vivo* performance of agro-food waste-derived bioactive glasses in various biomedical applications is critically evaluated. The chapter also investigates the effects of MgO and K_2O on the bioactive properties of different bioglasses and bioceramics. Finally, based on this comprehensive literature survey, motivation and specific objectives of the present work are outlined.

Chapter 3 details the synthesis of two glass series based on the nominal composition $43SiO_2$-$25CaO$-$25Na_2O$-$7P_2O_5$ (wt%). The first series involved the systematic substitution of CaO with MgO, resulting in the compositions $43SiO_2$-$25Na_2O$-$7P_2O_5$-(25-x)CaO-xMgO (where x = 0, 5, 10, and 15 wt%). The second series involved the substitution of Na_2O with K_2O, yielding the compositions $43SiO_2$-$25CaO$-$7P_2O_5$-(25-y)Na_2O-yK_2O (where y = 0, 5, 10, and 15 wt%). Both glass series were synthesized via the melt-quench method using

platinum-rhodium (Pt-Rh) crucibles. The chemical compositions of the as-synthesized samples were analyzed using energy-dispersive X-ray spectroscopy (EDS). Density measurements were performed using the Archimedes principle. Microhardness, a key mechanical property, was determined using a Vickers hardness tester. *In-vitro* bioactivity was assessed by immersing the glass samples in simulated body fluid (SBF) for various time periods (2, 5, 10, 20, and 40 days). Weight changes of the samples and pH changes of the SBF solution were monitored. The immersed samples were further characterized using XRD, FTIR, scanning electron microscopy (SEM), field emission scanning electron microscopy (FESEM) with EDS, and microwave plasma atomic emission spectroscopy (MP-AES) to investigate the physicochemical reactions occurring on the glass surface. Biocompatibility of the as-synthesized glasses was evaluated using the MTT assay on human peripheral blood mononuclear cells (PBMCs). Cell viability was measured using an ELISA microplate reader.

Chapter 4 presents the results obtained from the characterization of the synthesized glasses, followed by a detailed interpretation and discussion. The chapter is structured into four sections. The first section compares the properties of eggshells (ESP) as a calcium source with conventional $CaCO_3$. The second section details the results and discussion for the first glass series, $43SiO_2$-$25Na_2O$-$7P_2O_5$-(25-x)CaO-xMgO (where x = 0, 5, 10, 15 wt%). The third section investigates the effects of K_2O substitution for Na_2O in the control glass composition, focusing on the series $43SiO_2$-$25CaO$-$7P_2O_5$-(25-y)Na_2O-yK_2O (where y = 0, 5, 10, 15 wt%). The fourth section compares the properties of the hybrid glasses (derived from eggshells) with their counterparts synthesized using conventional precursors. The influence of MgO substituting for CaO and K_2O substituting for Na_2O is comprehensively studied using various characterization techniques. MgO substitution in the the glasses composition resulted in increased phase separation. Also, MgO plays a dual role, acting as both a network former (increasing polymerization within the silicate network) and a modifier in the phosphate network. On the other hand, K_2O substitution enhanced structural homogeneity and promoted the conversion of non-bridging oxygens (NBOs) to bridging oxygens (BOs), leading to a higher proportion of

odd-numbered Q^n units. Both MgO and K_2O substitutions widened the sintering window and improved thermal stability, with thermal expansion coefficient (TEC) suitable for biomedical coatings. Both modifiers increase the hardness as compared to control glass. The mixed modifier effect is also recorded in both series, exhibiting a non-linear trend through the different properties of glasses, as well as in *in-vitro* testing. *In-vitro* bioactivity tests revealed that all glasses formed carbonated hydroxyapatite (c-HAp). However, MgO substitution delayed c-HAp formation and Si^{4+} release while simultaneously improving cytocompatibility. Conversely, K_2O substitution accelerated c-HAp formation, with SNK-15 (15 wt% K_2O) showing the highest bioactivity, but reduced cytocompatibility over time due to increased ion leaching. Compared to their hybrid counterparts, conventionally derived glasses displayed higher density and hardness, more rapid and stable c-HAp formation, but lower fracture toughness and reduced cytocompatibility. The control glass, SC-0 (no MgO or K_2O substitution), demonstrated the most favorable balance of bioactivity and biocompatibility.

Chapter 5 concludes the results presented in chapter 4. In the end, future scope of the present study is given.

Chapter 1

Bioactive glasses: Classifications, applications and sustainable synthesis

Overview

This chapter provides a foundational overview of biomaterials and their diverse applications in modern medicine and healthcare. The main focus is on bioactive glasses and glass ceramics, a unique class of biomaterials with significant potential for tissue regeneration and repair. Key compositional modifications of bioactive glasses and their effect on bioactive properties are explored, highlighting how these variations can tailor material properties to meet specific clinical needs. Further, the mechanism to test the bioactivity and biocompatibility are discussed. Finally, the chapter introduces the concept of sustainable biomaterial synthesis using agro-food waste, setting the stage for further exploration of this promising area.

1.1 Biomaterials: An introduction

Biomaterials, encompassing natural and synthetic materials, are designed to interface with biological systems, replacing, supporting, or enhancing tissues and organs of living body [? ? ? ?]. These materials are used in a wide range of applications, from simple wound dressings and bone plates to complex devices like pacemakers and artificial hearts. A critical requirement for biomaterials is their ability to remain in contact with living tissues and body fluids for extended periods without causing adverse reactions [?]. This biocompatibility is achieved by mimicking aspects of living tissues, such as surface topography, porosity, and mechanical properties, ensuring a neutral response from the living body, free from inflammation or immune rejection.

The specific requirements for a biomaterial are dictated by its intended medical application. Implantable biomaterials, for instance, must meet more stringent criteria than those designed for external or temporary use. Major properties include biocompatibility, bioactivity, mechanical strength, and biodegradability [? ?]. As illustrated in **Fig. ??**, these properties are fundamental for ensuring long-term implant stability, functionality, and ultimately, patient well-being. Biocompatibility allows for harmonious coexistence with surrounding tissues, while bioactivity enables the materials to actively participate in biological processes like tissue regeneration. Mechanical strength is essential for withstanding physiological stresses, and biodegradability allows for controlled breakdown and absorption, especially crucial for temporary implants or scaffolds.

The biomaterials market is showing rapid growth, driven by the increasing demand for advanced healthcare solutions and the transformative impact of biomaterials on human health and longevity [? ?]. This growth, projected to reach a compound annual growth rate (CAGR) of 12.6% by 2032 from a market size of $123.8 billion in 2023, highlights the increasing integration of biomaterials in diverse medical devices, from heart valves and stents to joint replacements. Within this rapidly expanding field, bioactive glasses and glass-

ceramics have emerged as a prominent area of interest due to their unique potential in bone regeneration and tissue integration. This focus on bioactive glasses and glass-ceramics stems from their remarkable properties and ability to seamlessly integrate with living tissues, driving a significant increase in demand. Indeed, the market for these materials is now estimated to exceed 1.5 million units annually, with a value approaching $10 billion [? ?]. The choice of biomaterial, whether metal, polymer, ceramic, or composite, depends critically on the specific application and its functional requirements, underscoring the importance of ongoing materials science innovation in addressing the evolving challenges of medicine and healthcare. The following sections will delve deeper into the specific properties and applications of bioactive glasses and glass-ceramics, emphasizing their synthesis from sustainable resources.

1.2 Classification of biomaterials: based on biocompatibility

Biocompatibility, a material's ability to harmoniously interact with the body, dictates its integration with tissues and is crucial for success in specific applications. Biomaterials are classified into three generations based on their tissue interaction [? ?], as summarized in **Table ??**.

1.2.1 Bio-inert

Bio-inert materials represent the first generation of biomaterials and were designed to have minimal interaction with surrounding biological tissues when implanted into the body. These materials exhibit high chemical durability and resist degradation, maintaining their structural integrity in physiological environments. Due to their inert nature, they do not actively engage with the tissues and are often encapsulated by a fibrous layer of non-adherent tissue. Common examples of bio-inert materials include alumina (Al_2O_3), zirconia (ZrO_2), zirconia-toughened alumina (Zr-Al_2O_3), and yttria (Y_2O_3)[?]. The alloys and metals such as stainless steel and titanium, are widely used in orthopedic and dental applications due to their excellent mechanical properties,

corrosion resistance, and stability in both acidic and basic conditions. However, while bio-inert materials provide structural support, they do not integrate with the surrounding tissue and, in some cases, may lead to complications such as implant displacement or loosening strength over time [**?**].

1.2.2 Bio-active

The development of second-generation biomaterials in the 1970s marked a shift toward materials designed to stimulate specific biological responses at the interface with living tissues. This interaction promotes the formation of a strong bond between the material and surrounding tissue [**?**]. As a result, these biomaterials are referred to as bioactive due to their controlled reactions within the physiological environment. Examples of these bioactive materials include crystalline calcium phosphates, bioactive glasses, and bioactive glass ceramics. Clinically, these materials are widely used in applications such as bone regeneration, tissue augmentation, and as coatings on metallic implants to improve their integration with bone and enhance healing processes [**?**].

1.2.3 Bio-resorbable/Bio-degradable

Bio-resorbable/bio-degradable biomaterials represent the third generation of biomaterials, developed in the 2000s. Unlike other materials, which are unable to adapt to physiological load changes or biochemical stimuli, bio-resorbable biomaterials are designed to mimic the dynamic nature of living tissues [**?**]. This characteristic allows them to support the body's healing processes while gradually degrading over time. As the biomaterial is absorbed, it is replaced by natural tissue, thus enhancing the repair and regeneration of damaged areas. The development of these materials addresses the limitations of traditional artificial implants, providing a more biologically integrated approach to tissue repair and regeneration [**?**]. Nearly all calcium phosphates act as bio-resorbable materials. One of the important advantages of calcium phosphate biomaterials is that their dissolution products can be easily assimilated by the human body.

However, before the clinical implantation of any biomaterial, it is crucial

to carefully evaluate its biocompatibility and performance. Thorough testing is required to ensure that these materials not only interact with tissues as intended but also exhibit the necessary safety, efficacy, and longevity within the body. This evaluation process necessitates an approach involving various testing methodologies, as discussed in the following section.

1.3 Testing of biomaterials

Before implantation or use in human clinical applications, biomaterials must undergo thorough testing outside the body. Various testing methodologies, including *in-silico*, *in-vitro*, and *in-vivo* techniques, are utilized for this purpose. These preclinical tests are crucial for predicting how the material will interact with the complex biological environment of the human body and for identifying potential risks or limitations of the biomaterials. Such evaluations help ensure the safety, efficacy, and reliability of the biomaterial before clinical trials commence.

1.3.1 *In-silico*

In-silico testing, performed through computer simulations, is increasingly contributing to the biomedical field by predicting the behavior of pathogens, genes, and drugs within the human body. This approach allows for the rapid screening of therapeutic interventions, reducing the need for extensive physical trials and helping to streamline drug development. Additionally, it provides insights into complex biological interactions, accelerating the design of personalized medicine and improving patient health [**?**].

1.3.2 *In-vitro*

In-vitro testing is a critical step in the development and evaluation of biomaterials for potential clinical applications. These tests enable researchers to investigate the interactions of biomaterials with cells, tissues, and other biological components under controlled laboratory conditions. This provides an initial understanding of a material's biocompatibility, cytotoxicity, and bioactivity [**?**

].

The success of tissue engineering strategies depends on the ability to recreate or mimic the conditions of the healthy tissue. *In-vitro* tests, despite their usefulness, often lack the complexity of the human body, which includes a dynamic and multifaceted environment influenced by mechanical stimuli, vascularization, immune responses, and cellular interactions. For instance, *in-vitro* cytotoxicity tests provide valuable insights into immediate cell-material interactions, but they do not account for long-term responses such as chronic inflammation, degradation kinetics, or the material's behavior under physiological stresses. *In-vitro* methods cannot capture all complexities in the body during *in-vivo* tests as discussed in the following section. Despite these limitations, *in-vitro* testing remains an indispensable part of the evaluation process for medical devices, including implants. These tests precede *in-vivo* studies because they serve as valuable indicators of how newly developed biomaterials might behave when in contact with living tissue[**?**].

For biomaterials such as ceramics and bioactive oxide glasses, *in-vitro* testing typically involves cytotoxicity assays, such as the (3-(4,5-dimethylthiazol-2-yl)-2,5-diphenyl-2H-tetrazolium bromide) MTT assay, to assess the material's effects on cell viability and proliferation during degradation. Additionally, bioactivity is often evaluated by immersing the materials in different immersion mediums such as simulated body fluid (SBF), solution to observe both material degradation, and the formation of a hydroxyapatite (HAp)-like layer on the surface. This layer indicates the material's potential for bonding with bone tissue [**?**]. Before the development of SBF, *in-vitro* tests were conducted using distilled water or Tris buffer solution. The SBF solution synthesized by Kokubo et al. [**?**] mimics human blood plasma, with ionic concentrations more or less similar to those found in plasma (as given in **Table.??**).

For the synthesis of SBF during *in-vitro* studies, the pH of the solution is maintained between 7.25-7.4 at normal body temperature (37°C). Since Kokubo's innovation of SBF, several variations, such as revised SBF (r-SBF), modified SBF (m-SBF), and conventional SBF (c-SBF), have been proposed to

evaluate the *in-vitro* bioactivity of different materials [**?**]. Despite these alternatives, Kokubo's protocol remains widely used for testing *in-vitro* bioactivity. The SBF method is an efficient way to assess the bioactivity of materials like glasses [**? ?**], particularly for monitoring formation hydroxyapatite (HAp) on their surfaces. However, the bioactivity and HAp formation are highly dependent on the material's composition, processing parameters and their properties. For example, silicate-based bio-active glasses and glass-ceramics, including diopside-based ceramics ($Ca_2MgSi_2O_6$), have demonstrated excellent apatite-forming abilities in SBF [**?**]. Thus, the *in-vivo* bioactivity of these glasses and glass-ceramics can often be reliably inferred from their reaction in SBF [**?**]. In addition to this, the structure of the test samples, play a crucial role in validating the accuracy of *in-vitro* bioactivity tests. Additionally, *in-vitro* methods using tissue or cell cultures are also employed to assess the biocompatibility of bioactive glasses and glass ceramics.

1.3.3 *In-vivo*

In-vivo testing is performed within living organisms under controlled physicochemical conditions to observe biological responses in a natural environment. It is most commonly applied in animal testing to evaluate safety, efficacy, and potential side effects before proceeding to clinical trials involving human participants. This method provides valuable insights into the interactions between biomaterials and complex biological systems, helping to ensure the material's suitability for clinical biomedical applications [**?**].

1.4 Mechanism of bioactivity

In-vitro testing of biomaterials such as bioactive glass and glass-ceramics focuses on the formation of a HAp layer on the material's surface upon interaction with SBF. This HAp layer, specifically its carbonated form (HCA or carbonated (c-HAp)), is crucial for bonding with bone tissue due to its similarity to bone's mineral composition [**?**].

The process begins when the glass surface comes in contact with SBF, initi-

ating a series of chemical reactions. These reactions can be broadly categorized into leaching, dissolution, and precipitation [? ?]. Initially, alkali and alkaline earth metal ions (e.g., Na^+, K^+) from the glass network exchange with hydrogen ions (H^+ and H_3O^+) from the SBF, increasing the solution's pH level >7, resulting in increased basicity of the solution. This process is relatively easy because these ions function as modifiers in the glass network and are only weakly bonded to the network [?]. Further, the ion exchange reaction weakens the glass network, making it susceptible to dissolution. Hydroxyl ions (OH^-) then attack and break down the silica network ($-Si-O-Si-O-Si-$) of glasses and glass ceramics, releasing silicic acid ($Si(OH)_4$) into the solution. The release of the silica into the solution is highly dependent on the composition of the glass. [? ?].

Subsequently, the silicic acid undergoes polycondensation, forming a silica-rich gel layer on the glass surface. Calcium (Ca^{2+}) and phosphate (PO_4^{3-}) ions from the glass and the SBF then migrate to this silica-rich layer, precipitating and forming an amorphous calcium-phosphate (Ca-P) layer. Finally, carbonate ions (CO_3^{2-}) from the SBF incorporate into the Ca-P layer, leading to the crystallization of a c-HAp layer. The time required for HAp formation varies based on factors such as the material's composition, ion exchange rate, hydroxylation, and solution pH. Hench et al.[?] have detailed a five-step reaction sequence for c-HAp layer formation on glass surfaces, as given below [? ?] and shown in **Fig.1.1**:

- **Ion exchange:** Rapid exchange of alkali or alkaline earth metal ions (Na^+, K^+) with H^+ or H_3O^+ from the solution.

$$Si-O-Ca^{2+}+H^+ \rightarrow Si-OH^- + Ca^{2+} \tag{1.1}$$

- **Dissolution of silica:** Hydroxyl ions break $-Si-O-Si-$ bonds, forming silanols (Si-OH^-).

$$Si-O-Si+H_2O \rightarrow 2Si-OH \tag{1.2}$$

- **Silica re-polymerization**: Condensation of Si-OH^- groups forms a silica-rich layer.

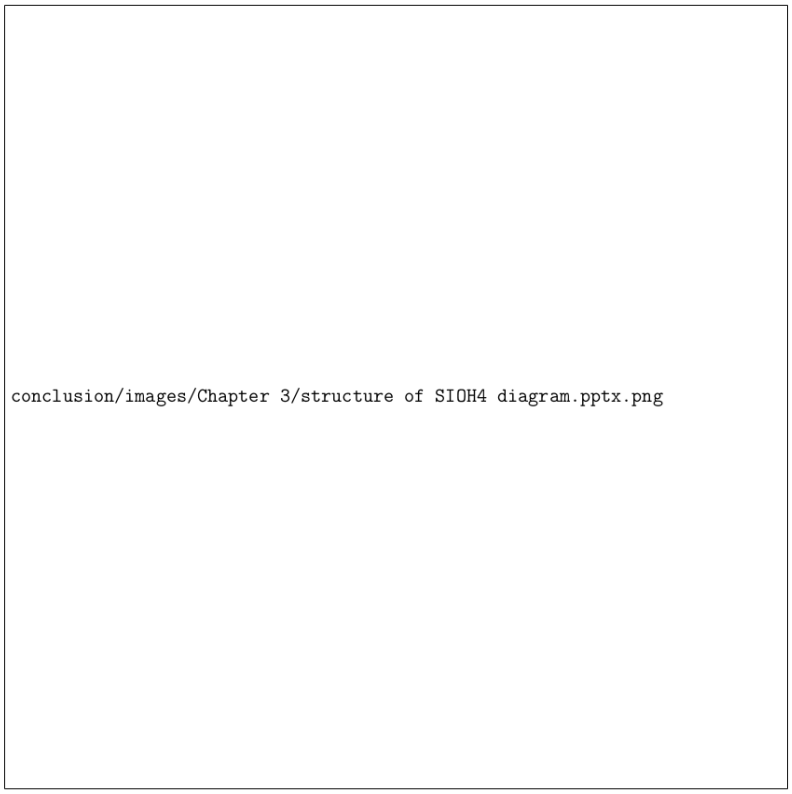

- **Ca-P layer formation:** Ca^{2+} and PO_4^{3-} migrate to the surface and form an amorphous Ca-P film.
- **HAp crystallization:** Incorporation of OH^-, CO_3^{2-}, or F^- and crystallization of the Ca-P layer into c-HAp or fluorapatite.

While the initial five steps of bioactive glass interaction—ion exchange, network breakdown, silica re-polymerization, Ca-P layer formation, and HAp crystallization occur independently of the surrounding tissues, they are essential prerequisites for subsequent tissue integration. The resulting c-HAp layer provides a scaffold for the next stage of biological interaction, which involves a

Figure 1.1: Mechanism of bioactive glass surface modification in response to SBF

cascade of reactions (steps 6-11), which include cell colonization, proliferation, and differentiation to form new bone with good mechanical bond to the implant surface [**?**]. These biological processes include cell colonization, proliferation, and differentiation, ultimately leading to the formation of osteoblasts and the growth of new bone tissue firmly bonded to the implant surface. Bioactive glass's effectiveness in regenerating soft tissues and hard tissues is intrinsically linked to the glass's structural properties and chemical composition as discussed in the following sections.

1.5 *In-vitro* cytotoxicity testing of bioactive glasses

While *in-vivo* testing provides the most comprehensive assessment of biomaterial performance within a living organism, *in-vitro* methods offer valuable preliminary insights and reduce the reliance on animal testing. *In-vitro*, cytotoxicity tests are particularly crucial for evaluating the biocompatibility of newly developed biomaterials like bioactive glass/glass ceramics [**?**]. These tests offer rapid, standardized protocols, generating comparative data that can identify and eliminate toxic materials early in the development process.

The most common *in-vitro* biocompatibility test utilizes cell cultures to assess various aspects of cell behavior, including cytotoxicity, proliferation, adhesion, and death. Cultured human and animal cells provide a controlled environment for evaluating the material's effects on cell viability and function. These studies are often referred to as cytocompatibility tests when focusing on one or two specific cell types [**?**]. Several methods exist for exposing cells to the test materials. In direct contact tests, the cells are cultured directly on the bioglass surface. Indirect contact tests employ an agar layer or filter between the cells and the material, while elution tests expose cells to the dissolution products released by the bioglass into the culture medium [**?**].

The choice of cell type significantly impacts the assay's performance and depends on the specific assay being performed as well as the laboratory's capabilities. Both primary cells and established cell lines can be used, derived from various tissues and organisms (animal or human). The selection of appropriate cell types for in vitro testing is guided by the intended application of the biomaterial [**?**]. For example, when evaluating a material designed for bone regeneration, human osteoblast cell (HOB) lines are commonly used. Osteoblasts, the single-nucleus bone-forming cells responsible for synthesizing and depositing HAp within the organic matrix, play a vital role in building strong, dense bone tissue [**?**].

Another important parameter is the time duration of the cell culture. While many tests are conducted over 24 hours, slower-growing cells like HOBs often

require longer culture periods, ranging from 3-7 days. In these cases, cell proliferation and spreading assays, frequently performed using 96-well plates, are employed to assess the biomaterial's influence on cell growth. One such assay, the MTT (3-(4,5-Dimethylthiazol-2-yl)-2,5 diphenyl tetrazolium bromide) assay, is a sensitive and reliable colorimetric method used to quantify cell proliferation, viability, and cytotoxicity[?].

The MTT assay provides a quantitative measure of cell viability, a key indicator of biomaterial cytotoxicity. In this assay, viable cells with active mitochondria reduce the yellow tetrazolium MTT salt to an insoluble purple formazan product by metabolically active cells. This reaction, catalyzed by succinate dehydrogenase, leads to formazan accumulation within the cells. **Fig. ??** illustrates the principle of the MTT assay, a common method for assessing cell viability. This color change, measured spectrophotometrically, provides a direct indication of the number of viable cells. Adding a solvent such as spectrophotometric grade dimethylsulfoxide (DMSO) or isopropanol dissolves the formazan, enabling colorimetric quantification, which directly corresponds to the number of viable cells. Cytotoxicity is then calculated as the ratio of viable cells to the total number of cells initially seeded. A biomaterial is generally considered cytocompatible if cell viability exceeds 70%. Since cytotoxicity is a primary concern for biomaterials intended for *in-vivo* use, the MTT assay plays a crucial role in assessing their safety. Furthermore, the MTT assay can reveal the impact of a biomaterial's structure on cell behavior, as ion release and subsequent pH changes can influence cell attachment, proliferation, and growth[? ?].

1.6 Bioactive glass and glass-ceramic: Properties and applications

Following the discussion of biomaterials and their classification, this section focuses specifically on bioactive glass and glass-ceramic as a unique class of biomaterials. As discussed in the above sections, ceramics and bioactive glass-based biomaterials form a specialized category of biomaterials that have a pro-

found positive impact on human beings or living [? ? ?]. The term "bioactive glass" refers to glass materials that are non-carcinogenic, non-antigenic, and compatible with surrounding tissues [?]. Bioactive glasses and ceramics offer superior biocompatibility, along with anti-corrosion and anti-compression properties, and possess composition flexibility that allows for tailored medical applications. Typically, these materials are brittle and mechanically strong, with elastic moduli similar to human bone. These materials are considered advanced materials for bone tissue engineering due to their ability to promote osteoprogenitor differentiation, enhance enzyme activity, support osteoblast cell adhesion, and aid in revascularization, making them ideal for bone regeneration and repair [?].

1.6.1 45S5 Bioglass®: A pioneering bioactive material

The second-generation biomaterial, bio-active glass known as "45S5 Bioglass®" was first designed by Larry L. Hench in 1969. The 45S5 Bioglass contains 45% SiO_2-24.5% CaO-24.5% Na_2O-6% P_2O_5 in weight% [?]. This glass demonstrates a positive response in living bone by triggering osteogenesis through the release of biologically active ions. The bioactivity of the glass can range from surface bioactivity to bulk degradability, allowing it to be resorbed within 10 to 30 days in tissue. The invention of Bioglass® revolutionized biomaterials development and led to the creation of doped bioactive glass systems for human being betterment. While ancient civilizations utilized biomaterials for reconstructing damaged body parts, Bioglass® has been in clinical use since 1985, particularly in dental applications, such as NovaMin and Perioglass.[? ?].

1.6.2 Compositional modifications and diverse applications

Bio-active materials, by definition, are designed to induce target-specific biological responses. A key advantage of bio-active glasses, which has attracted significant attention from researchers, is that even small changes in their chemical composition can lead to substantial changes in their properties. The performance of bioactive glass depends on its composition and structure. For

instance, Hench's 45S5 glass is a silicate (SiO_2)-based glass having short-range order (~ 3.4 Å) with alkali and alkaline ions such as calcium (CaO) and sodium (Na_2O) as modifiers and phosphorus pentaoxide (P_2O_5) as another glass network former oxide. The presence of a SiO_2 network promotes the formation of an HAp layer, which is essential for bonding with bone. The CaO and P_2O_5 release stimulates osteogenesis, while Na_2O enhances degradation, making it ideal for rapid bone boding and repairing [**?**].

Since the invention of bioglass, researchers have explored various compositional modifications to tailor bioactive glasses for specific applications. **Table ??** presents some examples of these modifications derived from the original 45S5 bioglass [**?** **?** **?**]. Modified bio-active glasses such as 13-93, 45S5F, and 58S are also employed in various biomedical applications, including dental repairs, knee replacements, and middle ear bone reconstruction, benefiting millions of patients worldwide. These advancements in bio-active glass compositions not only enhance their therapeutic potential but also make them attractive candidates for producing scaffolds used in bone regeneration [**?** **?** **?** **?** **?**].

Bioactive glasses, categorized as class A or class B based on composition, offer a versatile platform for biomedical applications. Class A bioglasses, primarily composed of SiO_2, CaO, and Na_2O, with potential additions of P_2O_5, CaF_2, or B_2O_3, exhibit high bioactivity, readily forming a hydroxyapatite (HAp) layer upon interaction with body fluids, leading to strong bonding with bone tissue. This controlled degradation and ion release stimulate bone regeneration, making them suitable for bone regeneration, tissue engineering, and dental restorations. Conversely, class B bioglasses, with higher silica content (over 60 wt%) show only osteoconductive properties and often incorporate biocompatible minerals like fluorapatite or wollastonite, are generally bio-inert, lacking the inherent ability to bond with bone. However, their structural stability and potential for composite formation, where bioactive phases can be integrated, make them valuable components in various biomedical applications [**?**].

Notably, research has revealed that modifying the composition of bioactive glasses, such as replacing Ca^{2+}, Na^{+} or creating phosphate-free variations, can

significantly alter their properties and bioactivity. For instance, incorporating MgO can enhance mechanical properties, thermal properties, biocompatibility, and biodegradability, while the addition of Al_2O_3 or B_2O_3 can influence surface reactions and formation of glasses, particularly reduces the melting temperature of the glass composition [**?** **?**]. Further tailoring of bioactivity and antimicrobial properties can be achieved by incorporating ions like Sr^{2+}, Cu^{2+}, Ag^{1+}, Zn^{2+}, and F^{1-}. This compositional flexibility highlights the adaptability of bioactive glasses for diverse biomedical applications, emphasizing the importance of understanding the interplay between composition, structure, and bioactivity for optimized functionality [**?** **?** **?**].

In addition to the composition, bioactive glass must have good interaction with body fluids, ensuring the formation of an apatite-like layer that promotes osteogenic cell proliferation and cellular adhesion, leading to partial bone replacement after long-term implantation. The synthesized glasses should also exhibit compatibility with host tissues without adverse effects. During synthesis, it's crucial to ensure that released elements remain within biologically safe levels, demonstrating compatibility and no cytotoxicity. **Fig.??** illustrates the ideal characteristics required for bioactive glasses as implants and their applications.

While traditional methods for synthesizing bioactive glass depend on conventional chemicals, researchers are increasingly looking for ways to synthesize these materials in a more sustainable, cost-effective, and eco-friendly ways. One exciting approach is to transform waste from agriculture and food production into bioactive glass. This "trash to treasure" approach not only holds promise for a greener future but also offers a potential solution for managing the vast amounts of agro-food waste generated globally.

1.7 Agro-food waste as resource

The global conflict from 1939 to 1945, highlighted the urgent need for increased food production and distribution to address widespread hunger and malnutrition. In response, the government in the post-war era prioritized revitalizing

the agricultural sector, paving the way for the Green Revolution. This initiative, combined with expanding farmland and a rising population, has resulted in a remarkable surge in agricultural output, which has more than tripled over the past 50 years. However, as agricultural production intensifies to support a growing population, managing agro-food waste has become a critical issue. The agricultural and food sectors generate approximately one billion tonnes of waste annually, with around one-third of all food intended for human consumption going unused or wastes[**?**]. This represents a complex challenge with significant environmental and economic impacts.

Although agricultural waste is biodegradable, the decomposition process can be slow, and farmers often need to clear their fields quickly for the next planting season. The costs involved in collecting, processing, and transporting this waste can be prohibitive, often outweighing potential profits from alternative uses. Consequently, some farmers burn crop residues, a practice that contributes to air pollution and produces ash as a secondary byproduct [**?** **?**]. Land-filling is another common disposal method, but it poses environmental risks such as greenhouse gas emissions and groundwater contamination[**?**]. The need for sustainable and efficient agro-food waste management is clear. Developing innovative approaches to reduce environmental impact while enhancing resource recovery is essential for planetary health and food security.

The agricultural industry, a major biomass producer, plays a key role in transitioning to a more sustainable energy future. Agricultural residues can be converted into biofuels like bio-oil, bio-char, and biogas, providing cleaner alternatives to fossil fuels and helping reduce greenhouse gas emissions [**?**]. However, the process of generating bioenergy from agricultural waste often leaves behind ash, a byproduct that requires careful management. While ash can be harmful due to its small particle size, it also contains valuable minerals like SiO_2, CaO, Na_2O, K_2O, and P_2O_5, making it a potential source for various value-added products[**?** **?**]. The mineral composition of agro-food waste ash varies depending on factors like crop type, soil composition, and fertilizer use, allowing for the synthesis of a diverse range of glasses and ceramic materi-

als. **Table ??** indicates the chemical compositions of different agro-food waste ashes, such as rice husk ash (RHA), sugarcane leaves ash (SCLA), sugarcane baggase ash(SCBA), corn husk ash(CHA), eggshell (ES), coconut cell (CC), peanut shell (PS), and wheat straw ash (WSA) residues, etc. [? ?].

RHA and ES are standout resources among agro-food waste ashes due to their composition and abundance. Rice husk, a common global byproduct, generates approximately 18-22 % RHA after processing, providing an economical, readily available, and highly reactive silica source with a substantial surface area [?]. Similarly, eggshells, which make up a considerable portion of global food waste, are rich in calcium carbonate ($CaCO_3$) and serve as an excellent calcium source for various applications [? ?].RHA, rich in amorphous silica (SiO_2) [?], can be obtained from rice husk through combustion or chemical extraction methods [? ?]. Typically, combustion-derived RHA comprises around 97 % silica, with trace elements making up the balance, and its purity can be further increased to nearly 99 % with acid or alkali treatments. On the other hand, ES, primarily composed of $CaCO_3$, can often be used directly as a raw material without significant pre-treatment [? ?].

The abundance of SiO_2 in RHA and $CaCO_3$ in ES makes them ideal candidates for synthesizing calcium silicate-based materials, including glasses and bioglasses [? ?]. RHA serves as a cost-effective source of silica for producing various glasses, including microelectronic devices, dielectrics [? ? ?], and importantly, bioactive glass-ceramics [? ?]. RHA-derived glass-ceramics, mimicking the composition of Hench's 45S5 bioglass, have demonstrated promising bioactivity when tested in simulated body fluid [?], highlighting RHA's potential for creating biocompatible materials suitable for bone regeneration and tissue engineering.

ES has also shown promise as a valuable source of calcium for producing hydroxyapatite (HAp), a well-known bioactive material that supports bone growth and integration [? ?]. This reinforces the versatility of agro-food waste as a sustainable source for synthesizing a range of advanced materials with applications in healthcare and beyond.

This chapter has explored the fundamental aspects of bioactive glasses and glass ceramics, including their properties, synthesis, and biological interactions, emphasizing sustainable approaches like using agro-food waste as a resource to develop bioglass or bioceramics. These discussions underscore the expanding interest and innovation within this field. The next chapter provides a comprehensive review of recent advances in sustainably derived bioglasses and glass ceramics, focusing on developments from the past few years.

Chapter 2

Literature review

Overview

This chapter presents a comprehensive literature review on sustainable bioactive glasses, focusing on utilizing agro-food wastes as a source of valuable precursors. The review explores the potential of various agro-food wastes, including rice husk ash (RHA) and eggshell powder (ESP), as sustainable alternatives to conventional materials. It examines different processing techniques for extracting valuable materials from these wastes and discusses various synthesis methods employed for producing bioactive glasses and glass ceramics. The review also analyzes the structure-property relationships in these materials, emphasizing the impact of composition and processing parameters on bioactivity, biocompatibility, and mechanical properties of end products. Furthermore, it investigates the *in-vitro* and *in-vivo* performance of agro-food waste-derived bioactive glasses in various biomedical applications. Finally, the chapter identifies key research gaps and motivation of the present study. Based on these, the objectives for the present work are given at the end of this chapter.

2.1 Value added materials from agro-food waste ashes

The increasing generation of agricultural, food waste residues and their ash by-products poses significant health and environmental challenges. However, these wastes also offer a valuable source of materials, as discussed in Chapter 1. Agro-food wastes and their ashes contain substantial amounts of elements like carbon, silicon, magnesium, and potassium (Table **??**), providing a sustainable alternative to conventional chemicals used in glass synthesis. Silica (SiO_2) is a major component in many agro-food waste ashes, such as rice husk ash (RHA) making them attractive for silica-based applications [**?** **?** **?** **?**]. However, the purity and form of silica depend heavily on processing parameters. While RHA can yield 80-97% pure silica, it also contains other alkali and alkaline earth metal ions (Table **??**), offering flexibility in glass composition but posing challenges for precise control over elements content. These challenges can be addressed through mineral extraction techniques such as calcination at controlled temperatures or acid pre-treatments to these wastes.

The processing parameters, particularly temperature and duration, are crucial in determining the reactivity and crystalline structure of the extracted silica. Controlled rice husk (RH) combustion below 700 ^oC typically yields amorphous silica ash. Higher temperatures ($>$ 800 ^oC) generally result in crystalline ash, although amorphous silica can still be obtained with a shorter duration at these heat treatment temperatures [**?**]. Fernandes et al. [**?**] reported the transition to crystalline silica above 850 ^oC. In a subsequent study, the two different extraction methods were used, and crystalline SiO_2 (cristobalite and tridymite phases) with approximately 99% purity was obtained after heat treatment above 1000 ^oC [**?**]. Some studies have achieved amorphous silica at temperatures up to 900 ^oC with heat treatment times less than 1 hour [**?**]. Conversely, prolonged exposure (e.g., 15 hours) can induce crystallization even at lower temperatures like 300 ^oC for heat treatment of RH [**?**].

Beyond temperature and time, pre-treatments like acid leaching can significantly influence the extracted silica's quantity and purity. For example, acid

leaching of RHA sintered at 600 °C under an inert atmosphere can yield silica >90% with few metallic impurities. Yalcin and Sevinc [?] and Real et al. [?] obtained silica from RHA with a purity index of 99.87% ± 0.01 by combining acid pre-treatment with burning RH at 700 °C for 6 hours in air. Deshmukh et al. [?] extracted amorphous SiO_2 with 97.73% purity using acid leaching followed by burning at three different temperatures. Dhaneshwara et al.[?] achieved similarly high SiO_2 purity (≈ 99%) by burning rice husk at 700 °C in an electric furnace followed by acid treatment. Beyond RHA as a rich silica source, food waste like eggshell powder (ESP) offers a valuable source of calcium. High-temperature treatment of ESP yields highly pure calcium oxide (≈ 99%) along with some trace elements [? ?]. Incorporating ESP into glass compositions introduces calcium oxide, which acts as a network modifier and can reduce the melting temperature of the glass melt, offering another avenue for tailoring material properties [?].

2.2 Biogenic silica derived bioglass/bioglass-ceramics

As discussed in the preceding section, agro-food waste ashes, rich in various minerals, have found applications in diverse engineering and medical fields. For glasses intended as biomaterials, *in-vitro* bioactivity testing, particularly the formation of a bone-like apatite layer on the material's surface when immersed in simulated body fluid (SBF), serves as a crucial evaluation method. This formation of the apatite layer, a key indicator of bioactivity, is influenced by several factors, including glass composition, the synthesis method, immersion time in SBF, and specific immersion conditions. Since the discovery of bioglass in 1969, researchers have extensively explored variations in composition and processing parameters to optimize bioactivity, according to the needs of different applications [? ? ? ?].

Beyond conventional chemical precursors, researchers have investigated the use of extracted silica from rice husk ash (RHA) as an alternative sustainable resource [? ? ?]. Various processing techniques, including sol-gel and melt-quench methods, have been employed to synthesize bioactive glasses using silica

derived from RH and RHA [? ? ?]. For example, Nayak et al. [?] extracted amorphous silica from RH as sodium silicate and utilized it as a source for synthesis of bioceramics. Similarly, Yucel et al. [?] synthesized 46S6 bioactive glass ($46SiO_2$-$24Na_2O$-$24CaO$-$6P_2O_5$ wt%) via melt-quenching at 1400 °C using biogenic silica from RHA. The glasses were immersed in SBF for 7 days at a concentration of 20 mg/ml. The result indicates the partial HAp formation, highlighting the influence of factors like surface area/volume ratio on apatite layer formation kinetics.

Further research by Yucel et al.[?] explored the effects of substitution of strontium (Sr^{2+}) for calcium (Ca^{2+}) in a $45SiO_2$-$24.5Na_2O$-$14CaO$-$6P_2O_5$-$10.5SrO$ (wt%) bioglass composition synthesized via melt-quenching using RHA-derived silica. It was found that Sr^{2+}, due to its lower field strength compared to Ca^{2+}, creates a more loosely cross-linked glass network. This structural change resulted in increased bioactivity and a thicker apatite layer with an increase in the immersion time in SBF (7 to 21 days). Furthermore, these bioglasses exhibited continuous, though slow, weight loss for up to 7 days in Tris buffer solution, attributed to the release of Ca^{2+}, Na^{+}, Si^{4+}, and P^{5+} ions. This degradation behavior, along with a favorable pH range (7.4-8.2) for osteoblasts, offers additional evidence of the bioactivity of the materials [?]. Similarly, Karakuzu-Ikizler et al. [?] investigated substituting magnesium and alumina (up to 1 wt%) for CaO in 45S5 bioglass synthesized with RHA-derived silica. Their findings indicated enhanced hardness without compromising bioactivity, surpassing the apatite layer formation observed in bioglasses made with commercial or conventional silica. The addition of magnesium and alumina also improved the biodegradability of the commercial silica glasses. The impact of heat treatment on mechanical properties was explored by Leenakul et al. [?]. Enhanced mechanical properties were observed in 45S5 bioglass made with biogenic silica after heat treatment at different temperatures. The promising bioactive properties were retained. These studies highlight the potential for tailoring bioglass properties through compositional adjustments and processing techniques when utilizing RHA as a sustainable silica source. Subsequently, the heat treatment temperature and glass stability significantly influence the

bioactivity and mechanical properties of bioactive glasses and glass ceramics. Glass ceramics, produced through controlled crystallization (vitrification, nucleation, and crystal growth), can exhibit enhanced density, chemical durability, and mechanical strength. Potentially, compressive strength can be increased due to heat treatment effects such as particle rearrangement, mass diffusion to pores, and grain growth. However, fully crystallized glass ceramics can negatively impact bioactivity by decreasing dissolution rates and hindering apatite formation [**?**]. A balance between enhanced mechanical properties and bioactivity can be achieved by inducing partial, controlled crystallization, resulting in semi-crystalline phases. Successful controlled crystallization depends on heat treatment parameters, including heating rate, nucleation, crystallization temperatures, and heat treatment duration. Precise control over these parameters is crucial for achieving homogeneous microcrystalline glass ceramics with uniform microstructures and optimized mechanical properties [**?**].

For instance, Peitl et al. [**?**] studied the crystallization and SBF interaction of Na_2O-CaO-SiO_2 glasses and glass-ceramics with varying P_2O_5 content in glass composition. It was observed that these materials formed a carbonated hydroxyapatite (c-HAp) layer even after controlled crystallization at 550–700 °C. Fourier-transform infrared spectroscopy (FTIR) and inductively coupled plasma mass spectrometry (ICP) analyses revealed significantly faster c-HAp formation (8–35 hours) after SBF immersion compared to conventional bioactive ceramics, which typically require at least 7 days. This enhanced bioactivity in the above composition is attributed to two key mechanisms: the formation of a non-phosphate bioactive crystal phase ($Na_2Ca_3Si_3O_9$) and the rapid release of phosphorus ions from the crystal structure's solid solution. Remarkably, even phosphorus-free compositions formed a c-HAp layer by absorbing phosphorus from the SBF solution. Although crystallization increased the onset time for c-HAp formation, it did not hinder the overall bioactivity of the material.

Many studies have reported similar findings, generally indicating that increasing crystallinity in bioglass/bioceramics slows down the bioactivity [**?**]. On the other hand, some research even demonstrates enhanced bioactivity

in partially crystallized glass-ceramics, where two or more crystalline phases are present [?]. For instance, Loh et al. [?] reported that heat-treating CaF_2-CaO-Na_2O-B_2O_3-SiO_2 glasses at 700 °C to form glass-ceramics increased densification, microhardness, and fracture toughness while retaining bioactivity comparable to the pristine glass. Their *in-vitro* bioactivity studies, using phosphate-buffered solution (PBS) immersion, confirmed apatite layer formation, indicating physicochemical reactions between PBS and glass that promote bioactivity. Some studies have even demonstrated that 45S5 glass-ceramic containing combeite crystals with high crystallinity (up to 100%) can retain their bioactivity [? ?]. Similarly, Siqueira et al. [?] reported that the formation of wollastonite ($CaSiO_3$) and α-tricalcium phosphate ($Ca_3(PO_4)_2$) crystalline phases in a glass matrix increased bioactivity.

In addition to using conventional chemical precursors for the synthesis of bioglass/glass ceramics, numerous studies have investigated RHA-derived bioglass and glass ceramics. These studies often report comparable properties to conventionally synthesized materials. For instance, Nayak et al. [? ?] utilized RHA as a silica source for sol-gel derived glasses ($50SiO_2$-$25Na_2O$-25CaO mol%). It was found that heat treatment at 1000 °C yielded combeite and devitrite crystals with good mechanical strength. However, heat treatment at 1050 °C resulted in decreased strength. This was due to the formation of cracks in glass ceramics, attributed to thermal expansion mismatch between glass matrix and ceramics. The same group also fabricated porous bioactive ceramics from RHA-derived silica gel, achieving a mechanical strength of 27.5 $\pm$ 0.2 MPa with $\sim$ 25% porosity. The apatite formation was confirmed during *in-vitro* test. Leenakul et al. [?] observed a transition from amorphous to crystalline phases in melt-quenched 45S5 bioglass derived from RHA upon heat treatment at 650-1050 °C. Optimal mechanical properties were achieved at 1050 °C while maintaining bioactivity. Furthermore, mesoporous bioglass (MBG) was synthesized from RHA via the sol-gel method. The results showed promise for drug delivery and bone regeneration, exhibiting no cytotoxicity and effectively delivering an anticancer drug [? ?].

In addition to RHA, eggshell powder (ESP) is another valuable agro-food waste resource, rich in calcium oxide, for bioglass and bioglass-ceramic synthesis. The use of eggshells and their membranes as a CaO source has gained significant attraction. An *in-vivo* study showed enhanced angiogenesis and antibacterial activity in copper-doped bioglasses nanocoated with the eggshell membrane (ESM)[?]. Punj et al. [? ?] synthesized bioactive calcium silicate glasses from corn husk ash (CHA), sugarcane leaf ash (SCLA), and ESP, reporting enhanced bioactivity and osteointegration compared to mineral-derived glasses, with microhardness increasing with eggshell replacement (575–638 HV). The same group also synthesized diopside ($CaMgSi_2O_6$) from these agro-waste sources, demonstrating apatite formation and non-toxicity *in-vitro* [?]. Palakurthy et al. [?] synthesized bioactive SiO_2–CaO–Na_2O bioglass from eggshells and RHA, confirming bioactivity, HAp formation, and cytocompatibility.

Beyond these applications, ESP has also been utilized to synthesize various bioceramics. Choudhary et al. [?] synthesized akermanite ($Ca_2MgSi_2O_7$), diopside ($CaMgSi_2O_6$), and nanocrystalline larnite (Ca_2SiO_4) using ESP via sol-gel and mechanical milling methods. HAp formation on akermanite was observed by them after 7 days in SBF. Cell proliferation, osteogenesis, and angiogenesis were promoted, while osteoporotic bone regeneration was suppressed *in-vitro*. The synthesized diopside exhibited a bonding strength of approximately 350 ± 7 MPa and a fracture toughness of 4 ± 0.3 MPa [? ? ? ?]. Other studies have explored wollastonite ($CaSiO_3$), diopside, forsterite, and pseudo-wollastonite ceramics synthesized from RHA and ESP by heat treatment at various temperatures (870–1300 °C). Wollastonite glass-ceramics showed a greater propensity for HAp formation than pseudo-wollastonite due to enhanced degradability in SBF [? ?]. Loh et al. [?] reported that these materials, sintered at 700 °C, achieved excellent mechanical properties (5.34 ± 0.21 GPa microhardness, 2.99 ± 0.24 MPa·$m^{1/2}$ fracture toughness), comparable to human enamel while retaining bioactivity and biodegradability in PBS, although with a slower apatite formation rate.

These studies highlight the complex relationship between thermal behavior, heat treatment temperature, and bioactivity. Higher heat treatment temperatures often increase crystallinity, potentially reducing bioactivity due to decreased dissolution and permeability in SBF and other *in-vitro* testing fluids. For bioglass and bioglass-ceramics derived from agro-food waste, biodegradability (silica network dissolution and apatite formation) is also influenced by impurity oxides inherited from the rice husk ash [?]. RHA-derived bioactive glass-ceramics (R-SBgC) combined with polycaprolactone (PCL) using the thermally induced phase separation (TIPS) method have shown promising results as bioactive composite scaffolds. These scaffolds have enhanced density and compressive modulus, suitable for non-load-bearing bone substitutes [? ?]. Other bioactive materials like calcium phosphate and silicate-calcium ceramics are also being synthesized from agro-food waste, showcasing the versatility of these sustainable resources [? ? ?]. These studies demonstrate the potential of agro-food waste-derived bioactive glasses and glass-ceramics for various biomedical applications, particularly in bone regeneration, due to their promising bioactivity and biocompatibility. While bioactive glasses stimulate bone growth by promoting the formation of hydroxyapatite (HAp), the use of naturally derived HAp itself as a biomaterial is also a promising area of research, as discussed in the following section.

2.3 Formation of hydroxyapatite from natural sources

As discussed in the previous section, HAp plays a crucial role in the bioactivity of bioglasses and glass-ceramics. This naturally occurring calcium phosphate mineral exhibits excellent bioactivity and is a major component of both teeth and bone, readily bonding with natural bone tissue due to its similar chemical and structural composition [?]. However, the mineral composition of human bone differs slightly from stoichiometric HAp due to the presence of impurities like carbonate, chloride, fluoride, magnesium, and sodium. [?] Natural bone apatite contains approximately 3–8 wt% carbonate [?].

While commercially available calcium phosphate bioceramics such as tri-

calcium phosphate (TCP), biphasic calcium phosphate (BCP), and HAp are often expensive due to the required high-purity reagents, naturally derived HAp presents a cost-effective alternative [?]. Natural sources, including fish bone, bovine bone [? ?], coral [?], and oyster shells [?], can be processed to obtain HAp. Naturally derived HAp often exhibits enhanced bioactivity due to its inherent porosity [? ?]. In contrast, commercially synthesized HAp, often produced via hydrothermal synthesis or chemical precipitation methods, may lack essential trace elements like magnesium, sodium, potassium, silicon, strontium, and iron [?].

Coralline HAp, derived from the hydrothermal conversion of coral skeletons, has been used in biomedical applications [? ? ?]. However, the endangerment and slow growth of some coral species necessitate exploring alternative renewable sources. Avian eggshells, with a mineral composition similar to coral and readily available, have emerged as a promising candidate, particularly for maxillofacial and craniofacial surgery [? ?]. Similarly, Chicken eggshells, comprising about 11% of an egg's weight, consist primarily of calcium carbonate (94%), with smaller amounts of magnesium carbonate (1%), calcium phosphate (1%), and organic matter (4%). Importantly, it also contain trace elements like Na, Mg, and Sr, found in human bone, further supporting their potential as a biomaterial source [?]. Furthermore, chicken eggshells are being used to synthesize various calcium salts crucial for bone regeneration, including β-tricalcium phosphate (β-TCP), BCP, CaO nanoparticles, and HAp. These calcium salts, commonly used in biomaterials, enhance the osteoconductivity of the resulting materials by mimicking the inorganic components of native bone [?].

Chicken eggshells, a readily available biowaste resource, are rich in calcium carbonate (95-98% $CaCO_3$) and also contain trace elements such as Mg, Sr, Si, Na, and F, making them an attractive source for HAp synthesis. While these trace elements are present in relatively small amounts, it can influence the properties of the resulting HAp. Studies have shown that the presence of these ions, even at trace levels, can affect the lattice structure, vibrational

frequencies, and thermal stability of commercially synthesized HAp, potentially impacting its bioactivity and biocompatibility [?].

Several studies have investigated the use of eggshells for HAp synthesis, employing various processing techniques. For example, Ahmed et al. [?] demonstrated the synthesis of HAp from calcined eggshells. Their method yielded HAp with a combination of amorphous and crystalline phases and a Ca/P molar ratio of 1.69. The researchers observed that further heat treatment could enhance the crystallinity of the final product. Siddharthan et al. [?] explored a microwave processing method to synthesize nanocrystalline apatite from chicken eggshells, achieving varying Ca/P ratios (1.5, 1.60, and 1.67). These eggshell-derived HAp materials exhibited improved morphology, stoichiometry, thermal stability at higher temperatures, and enhanced osteoblast cell adhesion compared to some commercially synthesized HAp materials [?]. Importantly, it has been also observed that the presence of trace elements did not negatively affect the bioactivity and biocompatibility of the eggshell-derived HAp [?]. Similar results were obtained by Dumitrescu et al. [?], who synthesized hydroxyapatite powder from eggshells using a microwave-assisted hydrothermal technique. Their study compared the eggshell-derived HAp with commercially available bone-derived HAp materials, namely partially deproteinized porcine bone (Gen-Os®) and deproteinized cortical bovine bone (Bio-Oss®). The results indicated that the eggshell-derived HAp exhibited significantly higher mesoporosity, suggesting improved biomolecule adhesion and osteoconductivity, which are essential properties for bone regeneration.

The specific extraction process employed for obtaining HAp from eggshells plays a crucial role in determining the final material's properties, including the Ca/P ratio, crystallinity, phase assemblage, and particle size [?]. These properties, in turn, influence the bioactivity, biocompatibility, and overall performance of the HAp in biomedical applications. Ahmed et al. [?], in their earlier work, reported that calcination of eggshells at 900 °C for 30 minutes resulted in the formation of a single crystalline HAp phase. This calcined HAp exhibited spherical, hexagonal, and cylindrical shapes, as confirmed by scan-

ning electron microscopy (SEM) analysis. The crystallite size was found to be in the range of 30-60 nm, and the Ca/P molar ratio was 1.66. This highly crystalline single-phase HAp contrasted with the mixed amorphous and crystalline phases observed in uncalcined eggshells. In addition, Patel et al. [?] reported the synthesis of highly crystalline hydroxyapatite from eggshells using a combination of sonication and calcination. Their method resulted in improved cell viability, suggesting a greater biocompatibility for the synthesized HAp. Furthermore, Sultana et al. [?] developed a novel UV-mediated solid state method for the synthesizing of hydroxyapatite from eggshells without the need for thermal treatment. This innovative approach involved ball milling the eggshells, followed by UV irradiation at room temperature. It was indicated by their results that the HAp produced through this UV-mediated method exhibited admissible *in-vitro* bioactivity and no significant cytotoxicity. Microwave irradiation offers a rapid and efficient method for HAp synthesis. Krishna et al. [?] synthesized nanocrystalline HAp (N-HAp) with this method, achieving platelet-like morphology, high-temperature stability, and enhanced osteoblast cell adhesion. Ultrasonication followed by calcination at 600 ºC has also been used to produce N-HAp with comparable mechanical properties to commercial HAp, exhibiting enhanced in vitro bioactivity and biocompatibility. Microwave processing advantages include shorter processing times, high reaction rates, narrow size distribution, and high purity, making it suitable for applications such as implant coatings [?]. Furthermore, heat treatment at higher temperatures (1000-1150 ºC) can refine particle size and improve mechanical properties such as compressive strength, hardness, and fracture toughness.

Numerous other methods, including wet chemical, solid-state reaction, hydrolysis, and mechanochemical techniques, have been employed for HAp synthesis [? ? ? ?] Ramesh et al. [?] used a solid-state sintering method with calcined eggshell powder (ESP) and dicalcium hydrogen phosphate dihydrate (DCPD), achieving high densities ($> 98\%$) at heat treatment temperatures of 1300–1350 ºC. Optimal properties, including enhanced fracture toughness and hardness, and a fine grain size, were obtained at 1250 ºC. Ho et al. [?] used a similar method, initially obtaining β-TCP with minor HAp, converting to

single-phase HAp after further heat treatment. These HAp/TCP bioceramics find applications in bone grafts, drug delivery, and protein purification.

2.4 Compositional and processing parameters effects on glasses and bioactivity

The properties of bioactive glasses and glass ceramics are intricately linked to their composition, structure, and processing methods. Synthesized primarily through melt-quench or sol-gel techniques, these materials are extensively used in biomedical applications, such as implant coatings, bone grafts, and scaffolds, where mechanical and thermal properties are crucial. Understanding the structural transformations and crystalline phases resulting from heat treatment is essential for optimizing their performance [**?**].

The glass transition temperature (T_g) is a fundamental parameter influencing the thermal behavior of bioactive glasses. As O'Donnell [**?**] demonstrated, precise estimation of T_g enables the prediction of other temperature-dependent properties critical for processing, such as annealing temperature, fiber-drawing temperature, and heat treatment temperature. Moreover, T_g is directly linked to the network connectivity of the glass, which governs both its bioactivity and mechanical properties. In applications like implant coatings, maintaining the stability of glass properties is critical, as undesirable variations, such as changes in the TEC, can induce stress and strain within the material. Localized strain may affect the bioactivity and as well as other properties of the glass [**?**]. Additionally, a mismatch in the TEC between the substrate and coating material can lead to delamination or failure of the composite system [**?**]. Therefore, understanding the thermal behavior and temperature-dependent properties of bioactive glasses is imperative for selecting optimal compositions and ensuring reliable performance. Several theories have been proposed to elucidate the roles of various ions in bioactive glasses, focusing on aspects such as structure, ionic potential, and network connectivity [**?** **?** **?**]. However, these theories often neglect the complex interplay between MgO and P_2O_5, particularly their combined influence on bioactivity. While P_2O_5 is a well-established glass former,

MgO exhibits a dual nature, acting as both a network former and a network modifier depending on its concentration and the overall glass composition [?].

Magnesium, a vital mineral in the human body after calcium, sodium, and potassium, plays a crucial role in numerous physiological processes [?]. It is a key component of bone, dentin, enamel, muscle, and soft tissues, acting as a cofactor in over 300 enzymatic reactions. Magnesium's involvement in physiological functions includes bone development, protein synthesis, muscle contraction and relaxation, nucleic acid synthesis, Adenosine triphosphate (ATP) metabolism, and vitamin-D stimulation. Maintaining appropriate magnesium levels in extracellular fluid (0.7-1.05 mMol/L) is essential for these processes. Its higher concentration in the stratum corneum, the outermost layer of the epidermis, suggests a role in skin barrier function, epidermal differentiation, and proliferation [? ? ?]. Additionally, magnesium regulates active calcium transport, activates phagocytosis, and is involved in calcification processes within calcified tissues [? ?]. However, magnesium's role in bioactive glasses is complex and debated. Some studies suggest that high magnesium concentrations hinder apatite layer formation [? ?], while others report no significant effect [? ?]. This discrepancy highlights the need for further research to fully understand the influence of magnesium on bioactivity. Balamurugam et al. [?] synthesized a $55SiO_2$-26CaO-13MgO-$6P_2O_5$ (mol%) bioactive glass via the sol-gel method and observed rapid increases in pH and the release of Ca^{2+} and Mg^{2+} ions in SBF, indicating high reactivity and bioactivity. The formation of a silica-rich layer that subsequently crystallized to form hydroxyapatite was reported, further confirming the material's bioactivity. While CaO and MgO share similar properties, CaO consistently acts as a glass modifier. It occupies interstitial spaces within the glass network, increasing non-bridging oxygen atoms and reducing network connectivity in the glass. This structural modification by CaO contributes significantly to the properties and bioactivity of the glass. The presence of magnesium in the glass composition is also reported to promote cell adhesion and osteoblast proliferation [?].

Al-Noaman et al. [?] investigated the effects of partially substituting MgO

for CaO in bioactive glass coatings. The resulting changes in thermal properties, structure, and bioactivity in SBF were evaluated for the glasses. Their findings indicated that magnesium suppressed crystallization and decreased the thermal expansion coefficient, glass transition temperature (T_g), and softening temperature (T_s). Importantly, it was concluded that the glasses' ability to form apatite was not inhibited by magnesium, but rather the onset of apatite deposition was delayed. This suggests a nuanced role for magnesium in the bioactivity mechanism. Wetzel et al. [? ?] further investigated the effects of partially replacing CaO with MgO, confirming that magnesium addition up to a certain threshold did not hinder apatite formation. Additionally, a widening of the sintering window for bioactive glasses with increasing magnesium substitution was observed, offering potential advantages for processing and controlling material properties. Fiume et al. investigated the biological response of novel silicate bioactive glasses containing MgO. In one study [?], a 47.5SiO_2-10Na_2O-10K_2O-10MgO-20CaO-2.5P_2O_5 (mol%) glass demonstrated excellent pro-osteogenic properties and complete resorption within 3 months *in-vivo*, with new tissue formation. An earlier study by the same group [?] on a similar SiO_2-Na_2O-K_2O-MgO-CaO-P_2O_5 glass also showed excellent cytocompatibility and osteogenic effects *in-vitro* and *in-vivo*. Jha et al. [?] found that substituting MgO for CaO in a SiO_2-K_2O-CaO-MgO glass increased chemical durability, slowing ion release during *in-vitro* bioactivity tests, while increasing hardness (464-502 HV), comparable to bone. These studies highlight the potential benefits of incorporating MgO in bioactive glasses for bone regeneration. Expanding on this, Ikizler et al. [?] studied the effect of 1 wt% MgO addition to 45S5 bioglass synthesized with biogenic silica via melt-quenching. Enhanced hardness in both biogenic and commercial silica-based bioglasses was observed. Moreover, magnesium incorporation specifically improved the bioactivity and biodegradability of the commercial silica-based glasses. These results highlight the significant influence of both silica source and magnesium addition on bioglass properties.

Further studies have demonstrated that the addition of alkali oxides to bioactive glass compositions can offer several advantages, including lower melting

temperatures, leading to more economical production. Up to a certain concentration, alkali oxides also enhance glass solubility in aqueous media, promoting increased interaction between the host tissue and the biomaterial, a key factor for bioactivity. Moreover, the presence of alkali oxides can improve the thermal stability of bioglasses by suppressing crystallization, which in turn facilitates better sintering and control over the final material's microstructure [? ?]. Cannillo et al. [?] investigated a novel potassium-based bioactive glass (46.1SiO_2-2.6P_2O_5-26.9CaO-24.4K_2O mol%), inspired by 45S5 Bioglass ®, where K_2O substituted Na_2O. While the thermo-mechanical properties and *in-vitro* response were comparable to 45S5, the potassium-containing glass exhibited higher stability during enameling, avoiding crystallization, unlike 45S5. This suggests its greater suitability for producing glass coatings. Crovace et al. [?] explored the impact of Na_2O substitution with K_2O in a similar silicate glass system. A decrease in crystallization kinetics and viscosity was observed, with the 50Na_2O/50K_2O composition exhibiting the fastest densification, confirming the mixed alkali effect (MAE) on sintering kinetics. While HCA formation in SBF was unaffected, the osteogenic potential of pre-osteoblastic cells was enhanced.

Sinitsyna et al. [?] studied the broad range of K_2O substitution for Na_2O (0-100%) in S53P4 bioactive glass, also observing an MAE, particularly influencing thermal properties, most notably around 20% K_2O. Higher K_2O levels expanded the glass network, decreasing density and widening the thermal processing window. Ion release kinetics in TRIS and SBF showed varied trends depending on the substitution level, with single-alkali glasses exhibiting superior bioactivity compared to mixed-alkali compositions. Moderate K_2O substitutions (<40%) reduced bioactivity and thermal processing flexibility, while higher levels (>66%) enhanced processability but moderately decreased bioactivity. Fully substituted K_2O glass, however, exhibited low crystallization and promising bioactivity. Similarly, Zia et al. [?] investigated the impact of K_2O on the microstructure of a Na_2O-CaO-P_2O_5-SiO_2 ceramic system synthesized via heat treatment at 900 °C. Increased thermal stability and a decreased crystallization tendency with increasing K_2O content were observed, which can be

beneficial for promoting bioactivity *in-vitro*. The major crystalline phases identified were sodium calcium silicate ($Na_2Ca_3Si_6O_{16}$), combeite ($Na_2Ca_2Si_3O_9$), and wollastonite ($CaSiO_3$). These findings highlight the complex influence of K_2O substitution on properties and bioactivity, enabling tailored glass design.

2.5 Biocompatibility of bioactive glasses/bioglass-ceramics derived from agro-food waste

Biocompatibility is an essential requirement for biomaterials, especially those intended for implantation. *In-vitro* cytotoxicity testing offers a crucial initial assessment of bioglasses and glass ceramics, providing valuable safety data and informing subsequent *in-vivo* studies [**?**]. Yucel et al. [**?**] studied the cytotoxicity of rice husk derived 46S6 bioactive glasses with a concentration of 20 mg/ml on sarcoma osteogenic (SAOS-2) osteoblast-like cells cultured in Dulbecco's Modified Eagle Medium-F12 (DMEM-F12) media via MTT assay. 46S6 glass has shown no toxic effect during the test. Furthermore, the substitution of strontium in 45S5 bioactive glasses (using RHA) was also studied to determine their cytotoxicity via MTT assay. Strontium has been considered a promising incorporation agent to enhance the replication of preosteoblast cells and reduce osteoclast activity. The results have shown good metabolic activity and cell viability, due to the controlled degradation rate of strontium and silica ions in DMEM cell culture media determined by inductively coupled plasma-optical emission spectroscopy (ICP-OES). It has also been found that pH change also directly affects the growth of cells, metabolic activity, and membrane potential due to their acidic and basic properties. The fast increment in pH because of H^+ cation occurs due to more ion dissolution of the glass [**?**]. Palakurthy et al. [**?**] used the human osteoarcoma MG-63 cell lines to test the cytocompatibility of RHA and ESP based bioglasses (SiO_2-CaO-Na_2O) with different concentrations (1000-50 μg/mL) and compared to blank control via MTT assay. The cell viability has been observed at >70% even at a higher concentration i.e., 1000 μg/mL. These bioglasses have demonstrated no toxicity effect that can be used in biomedical applications.

Punj et al[?] studied the effect of diopside synthesized using CHA, SCLA, and ESP on MG-63 cell lines. Furthermore, the cytotoxicity of agro-food waste-derived glasses on similar MG-63 cell lines was studied, and the non-toxic effect of the glasses was reported even at a higher 10 mg/ml concentration [?]. The biocompatibility of biogenic silica nanoparticles (bSNPs) derived from RHA and sugarcane bagasse ash (SCBA) was also assessed by Athinarayanan et al.[?] using MTT assay on human lung fibroblast cells (hLFCs) at different concentrations of bSNPs (0, 25, 50, 100, 200, and 400 μg/mL). The cell viability >85% has been found for bSNPs even at a higher concentration of 400 μg/mL, indicating bSNPs are biocompatible amd may be applicable for biomedical applications.

These findings consistently support the biocompatibility of agro-food waste-derived bioactive glasses, even with compositional modifications. Kargozar et al. [?] synthesized magnesium (Mg)-doped bioglass (SiO_2–P_2O_5–CaO–Na_2O –MgO–K_2O (mol.%)) to use in bone reconstruction. Futher, Shoaib et al. [?]synthesized the mesoporous bioactive glass (MBG) with composition (SiO_2-CaO-Na_2O-K_2O-P_2O_5 mol %) by sol-gel method. Polyethylene glycol (PEG 6000) was used as a soft template. Similar research group studied the effect of Mitomycin C (Mc) loaded mesoporous bioactive glass nanoparticles (Mg-MBG NPs) on MG-63 cancer cells and reported that Mg-MBG alone has no anti-proliferative effect but the Mc-Mg-MBG demonstrated an IC50 value of 20.8 μg/mL and significant inhibitory effects on cancer cells.

The following table summarizes key studies on bioactive glasses and glass-ceramics, highlighting the use of sustainable resources like RHA and ESP as precursors. The table also includes studies investigating the effects of MgO and K_2O substitution on the properties of bioactive glasses.

2.6 Motivation of the study

The development of sustainable and biocompatible materials is a critical area of research in biomedical engineering, driven by the increasing demand for environmentally friendly solutions. Bioactive glasses, with their proven efficacy in

bone regeneration and tissue repair, have garnered significant attention. While extensive research has explored synthesizing bioactive glasses from conventional sources, utilizing agro-food waste as a sustainable alternative presents a compelling opportunity. This approach not only reduces environmental impact but also creates value from the wastes. As detailed in this literature review, considerable progress has been made in utilizing agro-food waste, particularly rice husk ash (RHA) and eggshell powder (ESP), as sustainable precursors for bioactive glass synthesis. These studies demonstrate the feasibility of producing bioactive glasses with comparable or even enhanced properties compared to conventionally derived materials. However, a significant gap exists regarding the systematic exploration of hybrid bioglass systems combining agro-food waste-derived (SiO_2, CaO) and conventional mineral oxides such as P_2O_5 and Na_2O. Existing research primarily focuses on using agro-food wastes either as the sole raw material or as silica sources alongside conventional oxides, with limited exploration of hybrid systems. To the best of our knowledge, no studies have reported bioactive glasses derived from both rice husk and eggshell powder as silica and calcium sources, respectively, with systematic variations of MgO substituting for CaO and K_2O substituting for Na_2O in 45S5 bioglass for biomedical applications.

This identified gap and the potential for developing novel bioactive glasses with tailored properties and improved sustainability are the primary motivations for the present study. This research aims to contribute to a more sustainable biomaterials industry while advancing innovative solutions for bone regeneration and tissue repair by systematically investigating the effects of these compositional modifications and utilizing readily available agro-food waste resources.

Based on the above observations and literature survey, the following objectives are proposed for the present study.

2.7 Objectives

- Synthesis and characterization of $43SiO_2$+(25-x)CaO+(25-y) Na_2O+xMgO+ yK_2O+$7P_2O_5$ (x= 0,5,10, and 15; y= 0, 5,10 and 15) (wt%) glasses.
- In-vitro synthesis and characterization of hydroxyapatite layer on developed glass and glass ceramics.
- Evaluation of cytotoxicity of selected glass and glass ceramics.

Chapter 3

Materials and methods

Overview

This chapter details the synthesis and characterization of calcium silicate glasses derived from hybrid resources, incorporating both agro-food waste (rice husk ash and eggshells) and conventional chemicals. The structural, thermal, microstructural, and physicochemical properties of the as-prepared glasses were investigated. Crucially, their bioactivity and biocompatibility, assessed using simulated body fluid (SBF) and human peripheral blood mononuclear cells (PBMCs), respectively, were evaluated to determine their suitability for biomedical applications. The synthesis procedure, characterization techniques, and testing methodologies, including the specific conditions and parameters for each analysis, are comprehensively described.

Agro-food wastes, such as rice husk ash and eggshells, represent a valuable source of materials with potential applications in various fields, particularly biomedicine. Careful selection and processing of these wastes are crucial for obtaining materials suitable for transforming them into valuable resources.

3.1 Agro-food wastes as raw materials

The present study aims to synthesize bioactive calcium silicate glass compositions from hybrid sources, that is, agro-food waste ashes and conventional chemicals. Rice husk (RH) was collected from a local rice mill in Patiala, Punjab, India. The obtained RH was initially cleaned to remove soil particles or remaining rice straws. Furthermore, it was washed with normal water to remove any remaining dust. The dried RH was used to obtain RHA. Further, RHA was calcined using two different heat treatments to obtain silica (SiO_2). The RHA was first calcined at 1250 ºC for 4 h (As shown in **Fig. ??**), followed by heat treatment at 1450 ºC for 4 h. Chicken eggshells (ES) were obtained from the hostel of the Thapar Institute of Engineering and Technology, Patiala, Punjab, India. The eggshells were washed with distilled water to remove impurities and kept in a 1M HCl solution for 2 h, followed by washing with distilled water. Then, ES were kept in the oven at 70 °C for 6 h to remove any moisture from the eggshell. Finally, eggshells were ground in an agate mortar to convert into powder.

The purity of SiO_2 and $CaCO_3$, determined using energy-dispersive X-ray spectroscopy (EDS) with Quantax Esprit software (Bruker microanalysis), was found to be 97.7 wt% and 98 wt%, respectively, with trace elements listed in **Table ??**. These sources, obtained from agro-food wastes and other required conventional chemicals according to the objectives, were used to synthesize the bioactive glasses. Details of the glass synthesis, characterization, and testing procedures are provided in the following sections.

Further, details of the glass synthesis are given in the following section.

3.2 Synthesis of bioactive glass

Bio-active glasses can be synthesized by using different techniques, such as melt quenching, sol-gel, chemical deposition, and co-precipitation etc. The first ever 45S5 bioglass was synthesized using the traditional melt- quenching method [**?**]. However, melt quenching and sol-gel are the well developed and prominent methods used for the preparation of bioactive glasses. Each and every technique has merit and demerit. In the present case, the conventional melt quench technique has been adopted to synthesize the glasses.

The first series of glass compositions was synthesized to study the effect of MgO substitution on bioactivity. The selected compositions were as follows: **43SiO_2-(25-x)CaO-(x)MgO-25Na_2O-7P_2O_5 (x = 0, 5, 10, and 15 wt%)**. The derived SiO_2 and $CaCO_3$ from RHA and ESP, respectively, were combined with the conventional chemicals (Na_2CO_3, P_2O_5, MgO) in the desired proportions. The conventional chemicals such as sodium carbonate (Na_2CO_3) with 99.99% purity (Loba Chemie), phosphorus pentoxide (P_2O_5-99.99%, Loba Chemie), magnesium oxide (MgO-99.99%, Loba Chemie) were used as the conventional chemicals. These were used without any further purification. The blended mixture of conventional chemicals and agro-food waste-derived SiO_2 and $CaCO_3$ was homogenized by grinding for 2 hours (h) in an acetone medium. To remove any residual carbonates, the mixture was calcined at 1000 °C for 2 h. The calcined material was then grinded again for 1 h. The grinded, calcined mixture was heated in a platinum-rhodium crucible within an electronic furnace (Okay model with $MoSi_2$ heating elements) at a rate of 5 °C/min. The mixture was held at intermediate temperatures (300 °C, 600 °C, 900 °C, and 1200 °C) for 0.5 h each to promote diffusion and minimize volatilization of certain components before finally being melted at 1550 °C. The melt was then air-quenched using two thick copper plates. The melt was air-quenched using two thick (6.84 mm) copper plates.

Second series of glass compositions was synthesized to investigate the effect ofK_2O in place of Na_2O. In this series, Na_2O was incrementally replaced with

K_2O in the following compositions: **$43SiO_2$-25CaO-(25-y)Na_2O-(y)K_2O-$7P_2O_5$ (y = 0, 5, 10, and 15 wt%).** The same procedure as described for the first series was used to synthesize these glasses. The nominal composition of all the glass samples along with their labels are given in **Table ??**

3.3 Characterization methods

3.3.1 Density measurement

Density is a crucial parameter that provides insights into the compactness, porosity, and interconnectivity of the glass structure [?]. This directly influences the bioactivity of glasses, affecting both their degradation rate and interaction with surrounding tissues. In the present study, density (ρ) of the as-quenched glasses was determined using Archimedes' principle with xylene using as buoyant medium:

$$\rho_{\text{sample}} = \frac{W_a}{W_a - W_x} \times \rho_{\text{sample}} \tag{3.1}$$

where ρ_{xylene} is the density of xylene (0.863 g/cm^3 at 30°C), W_a is the weight of the sample in air, and W_x is the weight of the sample in xylene. Subsequently, molar volume (V_m) and oxygen packing density (OPD) were derived from the calculated density using standard equations as given below:

$$V_m = \frac{M}{\rho_{\text{sample}}} \tag{3.2}$$

$$\text{OPD} = C \times \frac{\rho_{\text{sample}}}{M} \tag{3.3}$$

Where C is the number of oxygen atoms per formula unit.

3.3.2 X-ray diffraction (XRD)

XRD is a non-destructive technique widely used to characterize materials' structural properties, including identifying amorphous or crystalline phases. In the present study, the XRD was performed on the as-prepared samples as well as after immersion in simulated body fluid (*in-vitro* testing) to confirm

the amorphosity, nanocrystallinity, and hydroxyapatite (HAp) formation, respectively. The principle of XRD relies on the interaction of X-rays with the arrangement of atoms in a crystalline lattice [**?**]. This ordered arrangement creates planes with characteristic interplanar spacings (d-spacing). When X-rays interact with these planes, diffraction occurs according to Bragg's law:

$$2dsin\theta = n\lambda \tag{3.4}$$

where 'n' is the order of reflection, λ is the X-ray wavelength (0.1-4 Å), and θ is the diffraction angle. Constructive interference from diffracted X-rays results in diffraction peaks, which are analyzed to identify the crystalline phases. In a typical X-ray diffractometer, monochromatic X-rays are generated by a cathode ray tube, filtered by crystal monochromators, collimated, and directed onto the sample. As the sample and detector rotate, the intensity of reflected X-rays is recorded. When the incident X-rays' geometry satisfies Bragg's law, constructive interference occurs, producing diffraction peaks. A detector records and processes these X-ray signals, converting them into counts per second, and the output is displayed on a computer monitor (e.g., as shown in **Fig. ??**).

As the glasses lack long-range atomic order, they exhibit broad halo patterns in XRD instead of sharp diffraction peaks. The halo's position is composition-dependent, and multiple halo's may indicate phase separation or inhomogeneity [**?**]. In contrast, glass ceramics, which possess partial crystallinity, exhibit both broad halo and crystalline peaks embedded over the glass matrix. XRD analysis provides crucial information on the crystalline phases formed during heat treatment or after immersion in SBF, which is essential to understand the bioactivity of these materials.

In this study, XRD patterns were acquired using a Rigaku Smartlab SE X-ray diffractometer with a Cu-Kα source (λ = 1.54 Å). Measurements were performed in air over a 2θ range of 10-90° with a scanning speed of 4°/min and a step size of 0.02°. Phase identification was carried out using X'Pert

HighScore Plus software. Samples were analyzed in their as-quenched state, both before and after SBF immersion (*in-vitro* testing).

3.3.3 Differential thermal analysis (DTA)

DTA is a crucial technique for assessing the thermal behavior of materials, providing insights into thermal stability and phase transitions, such as the glass transition temperature (T_g) and crystallization temperature (T_c). These characteristic temperatures are essential for understanding material properties and processing parameters [**?**]. For bioactive glasses, T_g and T_c are particularly important as they influence the sintering and crystallization behavior during the fabrication of glass-ceramics, which can significantly impact the final material's bioactivity. Many processes, such as coating and enameling, involve subjecting the glass to high temperatures, often near or exceeding the crystallization temperature (T_c) [**?**]. Therefore, determining the thermal stability of the glass through DTA is essential.

In DTA, both the sample and an inert reference (e.g., Al_2O_3) are subjected to identical thermal cycles, and the temperature difference (ΔT) between them is continuously monitored. This difference is plotted against temperature, producing a DTA curve (thermogram). Endothermic and exothermic peaks on the thermogram correspond to physical or chemical changes in the sample, such as glass transition, crystallization, melting, and other phase transitions. A typical DTA setup (e.g., as depicted in **Fig. ??**) includes a furnace, sample and reference holders equipped with thermocouples, and a recording system. The differential arrangement of thermocouples, connected to a differential amplifier, allows for precise measurement of the temperature difference between the sample and reference, enabling the detection of even subtle thermal events.

In this study, DTA was performed using a Perkin Elmer Diamond Pyris TG/DTA instrument. Approximately 15 mg of glass powder was placed in a Pt crucible, with Al_2O_3 (99.9% pure) as the reference material. The T_g and T_c were determined from DTA curves obtained in the 20–1000°C range at a heating rate of 15°C/min. The softening temperature (T_s) was determined via

dilatometric measurements using a Netzsch DIL402PC dilatometer at a heating rate of 5°C/min in air. The temperature measurements were accurate to within ±1°C.

3.3.4 Scanning electron microscopy (SEM) and energy dispersive spectroscopy (EDS)

SEM, coupled with EDS, played a crucial role in characterizing the synthesized glasses and glass-ceramics before and after immersion in simulated body fluid (SBF). SEM generates high-resolution images by scanning a focused electron beam across the material's surface. The interaction of the electrons with the sample produces various signals, including secondary electrons (SE), backscattered electrons (BSE), and characteristic X-rays, which provide information about surface topography, elemental distribution, and composition, respectively [**?**]. A schematic of the SEM principle is shown in **Fig. ??**. Field emission scanning electon microscopy (FESEM) is a similar instrument to SEM; it provides enhanced resolution (down to 1.5 nm) up to three to six times better than conventional SEM and provides clearer and less distorted images [**?**].

EDS, integrated with SEM, provides elemental analysis of the sample. When the high-energy electron beam of the SEM interacts with the sample, it causes the ejection of inner-shell electrons from atoms within the sample, creating vacancies (as shown in **Fig.?? b**). These vacancies are quickly filled by outer-shell electrons, releasing energy in the form of characteristic X-rays unique to each element. An energy-dispersive X-ray (EDX) detector measures these X-rays, allowing for the identification and quantification of the elements present [**?**]. This is essential for verifying the composition of the synthesized glasses and confirming the presence and relative amounts of key oxides. In the context of bioactivity assessment, SEM-EDS is particularly valuable. After SBF immersion, SEM allows for direct visualization of hydroxyapatite (HAp) formation on the material's surface, providing insights into the morphology of the HAp layer, including its thickness, density, and crystallinity. EDS is crucial for determining the Ca/P ratio within the HAp layer, a key indicator of bone-bonding

potential. A Ca/P ratio close to that of natural bone apatite (approximately 1.67) is considered desirable for good bioactivity. Furthermore, SEM-EDS can be used to identify different phases formed in glass-ceramics, as well as to track elemental changes during degradation studies.

For the present study, SEM micrographs were obtained using a JEOL/EO SEM (version 1.0). Samples were coated with gold (Au) using a JEOL JEC-3000 FC auto fine coater at 20 mA for 60 seconds. Higher-resolution imaging was performed using a Zeiss Sigma 500 field emission scanning electron microscope (FESEM). Elemental analysis was conducted via energy-dispersive X-ray spectroscopy (EDS) using a Bruker Quantax XFlash 6130 detector on the FESEM, operating in low vacuum mode.

3.3.5 Fourier Transform Infrared Spectroscopy (FTIR)

Infrared spectroscopy is a crucial analytical technique in materials science, based on the principle of molecular vibrations. When infrared radiation interacts with a sample, specific wavelengths are absorbed, corresponding to the vibrational frequencies of the material's structural units, while the remaining radiation is transmitted. The infrared spectrum is broadly divided into three regions: far-infrared (< 400 cm^{-1}), mid-infrared (4000-400 cm^{-1}), and near-infrared (13000-4000 cm^{-1}). A change in the electric dipole moment during vibration is essential for infrared absorption. FTIR spectroscopy, the most common infrared method, employs the interference of two beams to generate an interferogram, a signal based on the path length difference between the beams. Fourier transformation converts this signal from the distance domain to the frequency domain (wavenumber). The resulting spectrum, displaying transmittance as a function of wavenumber, is then analyzed by assigning specific bands to the vibrations of distinct structural units. This unique spectral fingerprint allows for the identification of a sample's structural components and can even be used to evaluate bond strength. Overlapping bands can be resolved using deconvolution, a signal processing technique that enhances spectral resolution [**?**].

FTIR spectroscopy is particularly valuable for analyzing bioactive glasses and glass-ceramics, both before and after immersion in simulated body fluid (SBF). A key aspect of bioactivity is the formation of silanol groups (Si-OH^-) when exposed to physiological fluids. Network modifiers within the silica network disrupt the tetrahedral SiO_4 units, breaking Si-O-Si bonds and forming Si-O-NBO (non-bridging oxygen) groups. This process, coupled with silicate network dissolution, is crucial for bioactivity. FTIR spectroscopy, sensitive to these vibrational mode changes, provides insights into these structural transformations. Analyzing the Si-O-Si and Si-O-NBO absorption bands reveals information on network connectivity and the influence of modifiers [**?**]. Each glass composition's unique infrared absorption spectrum serves as a fingerprint, facilitating the identification and comparison of different structures. Comparing spectra before and after SBF immersion allows for identifying structural changes such as hydroxyapatite (HAp) formation or alterations in the glass network, which elucidates the bioactivity mechanism.

In this study, FTIR analyses were conducted using an IRTracer-100 spectrometer (Shimadzu Corporation, Japan). Spectra were recorded in the 400–4000 cm^{-1} range with a 2 cm^{-1} resolution using the KBr pellet method (0.5 mg sample mixed with 200 mg KBr). Data analysis, including deconvolution of overlapping bands, was performed using Origin 2018 software. The accuracy of the Gaussian fitting during deconvolution was assessed by maximizing R-squared ($R^2 > 0.999$) and minimizing reduced chi-squared ($\chi^2 \sim 10^{-7}$).

3.3.6 Vickers Microhardness

Vickers microhardness measurements were performed on the as-quenched samples using a Mitutoyo MVK-H0 microhardness tester (Japan) equipped with a diamond Vickers indenter. Indentations were made at four different points on each sample surface using an applied load of 100 gf for a dwell time of 15 seconds as shown in **Fig. ??**. . The indentations were made on the as-prepared sample surfaces without prior polishing. A light microscope (Eclipse-MA100, Nikon, Tokyo, Japan) at 100x magnification was used to measure the lengths of

both diagonals immediately after indentation. Three indentations were made at each of the four points to minimize error, and the average diagonal length was used for the calculations.

The Vickers microhardness (HV) was calculated using the following equation:

$$HV = \frac{1.854L}{d^2} \tag{3.5}$$

where L is the applied load in gram force (gf) and d is the average diagonal length (mm) of the indentation.

3.4 Characterizations for bioactive properties

In addition to the characterization techniques mentioned above, further analyses are necessary to explicitly confirm the bioactivity phenomenon discussed in this section.

3.4.1 *In-vitro* testing

In-vitro bioactivity and degradation of the powdered glass samples were assessed using simulated body fluid (SBF). The SBF solution was prepared according to Kokubo's protocol [?] using high-purity NaCl, $NaHCO_3$, KCl, $K_2HPO_4{\cdot}3H_2O$, $MgCl_2{\cdot}6H_2O$, $CaCl_2$, and Na_2SO_4 dissolved in deionized water. The pH was maintained at approximately 7.34 (within the normal range of human blood plasma) using 50 mM Tris-hydroxymethyl aminomethane-($(CH_2OH)_3CNH_2$) and 45 mM HCl. A weight (powder sample) to volume (SBF solution) ratio of 0.02 g/mL was maintained [? ?]. One gram of each glass powder was immersed in 50 mL of SBF in polyethylene bottles and incubated at 37 °C for 2, 5, 10, 20, and 40 days.

SBF pH was monitored daily using a digital pH meter (P Hep model HI96107, precision 0.1). Samples were collected after 2, 5, 10, 20, and 40 days of immersion, filtered, dried at room temperature, and weighed using a Mettler Toledo precision microbalance to determine weight loss (W_c) according to the following equation:

$$W_c\% = \frac{W_0 - W_f}{W_0} \times 100 \tag{3.6}$$

Where W_0 and W_f are the initial and final weights of the sample, respectively. Soaked samples were characterized using XRD, FTIR, and SEM-EDS and compared to pristine (unsoaked) samples. The residual SBF was analyzed using microwave plasma atomic emission spectroscopy (MP-AES) to determine the elemental release profile.

3.4.2 Microwave plasma-atomic emission spectroscopy (MP-AES)

MP-AES is a highly sensitive elemental analysis technique that is valuable in various applications. In the present bioactive study, MP-AES is used for the quantification of trace elements released from the samples, providing insights into the dissolution behavior of the material and corroborating observed changes in the pH of the SBF and the sample weight. A magnetron and a waveguide are major components of the instrument. The magnetron generates electromagnetic energy (3.5 GHz), which is transferred to a waveguide assembly and focused onto a plasma torch [**?**]. The sample, introduced into the plasma via a nebulizer, is atomized and excited by the microwave-generated nitrogen plasma. This excitation causes the atoms to emit light at characteristic wavelengths, which are then detected by the solid-state charge-coupled device (CCD) detector, and used to quantify the elemental concentrations, even at very low levels (parts per billion).In the present bioactive study, MP-AES serves as a complementary technique, providing detailed elemental release profiles (up to ppb levels) to corroborate the observed pH and weight changes in the immersed samples.

In the present work, an Agilent 4100 MP-AES system (spectral resolution: 25-40 pm) was used to quantify ion concentrations leached from the samples into SBF. Samples (0.1 g) were dissolved in 1N HNO_3 (10 mL) and water (25 mL), heated to reduce volume by 50%, and then diluted with 100 mL of water. All measurements were performed in triplicate and average values were used for final analysis.

3.5 Biocompatibility test

3.5.1 MTT assay

The cytotoxicity of all glass samples were evaluated using the MTT (3-(4,5-dimethylthiazol-2-yl)-2,5-diphenyltetrazolium bromide) assay with human peripheral blood mononuclear cells (PBMCs) [**?**]. PBMCs were isolated from healthy volunteer blood using density gradient centrifugation with HiSep™

LSM1077 (HiMedia, India), following the standard method. The isolated cells were washed with phosphate-buffered saline (PBS) and resuspended in Dulbecco's Modified Eagle Medium (DMEM, HiMedia, India) supplemented with 5% fetal bovine serum, 100 UI/mL penicillin, 100 µg/mL streptomycin, and 25 µg/mL amphotericin B. Cells were seeded in a 96-well plate at a density of 4 × 10^5 cells/well.The schematic illustration of the MTT assay is shown in **Fig. ??**.

For dose-response assessment, cells were treated with varying sample concentrations (0-200 µg/mL) for 24 h in a humidified incubator at 37°C with 5% CO_2. Based on these results, a concentration of 100 µg/mL was selected for time-dependent cytotoxicity assessment over 48 h. Following incubation, 200 µL of supernatant was removed, and 20 µL of MTT solution (5 µg/mL) was added to each well. After 4 h of incubation in the dark, 150 µL of DMSO was added to each well, and the absorbance was measured at 540 nm using an Infinite Pro ELISA reader. Cell viability was calculated relative to untreated controls:

$$\text{Viability (\%)} = \frac{\text{OD of treated cells}}{\text{OD of control}} \times 100 \tag{3.7}$$

Experiments were performed in triplicate with three independent biological replicates. Results are presented as mean ± standard deviation. Statistical analysis was performed using one-way ANOVA with Tukey's multiple comparison test (GraphPad Prism, GraphPad Software, Inc., San Diego, CA).

Chapter 4

Results and discussion

Overview

This chapter presents the synthesis, characterization, and *in-vitro* assessment of two bioactive glass series prepared via the melt-quench method. The first series investigated the substitution of CaO with MgO ($43SiO_2$-$25Na_2O$-$7P_2O_5$-(25-x)CaO-xMgO, x = 0, 5, 10, and 15 wt%) while the second explored the replacement of Na_2O with K_2O ($43SiO_2$-$25CaO$-$7P_2O_5$-(25-y)Na_2O-yK_2O, y = 0, 5, 10, and 15 wt%), initially using hybrid sources (eggshell and agro-food waste ash) combined with conventional chemicals. Different characterization techniques were used to determine the change in properties of the glasses before and after immersion in SBF. The MgO substitution improved the compactness and thermal stability, while K_2O decreased density and reduced phase separation. Both modifiers increased the sintering window and resulted in Vickers hardness values ranging from 4.65 to 6.2 GPa. *In-vitro* testing in SBF showed that MgO initially retarded but later stabilized HAp formation, while K_2O promoted faster c-HAp growth. All glasses exhibited good cytocompatibility (>85% cell viability). All glasses indicate good cytocompatibility (MTT assay with PBMCs) with >85% viability. Based on the results, the best glasses were synthesized using only conventional precursors for comparison. The results indicate a higher hardness and faster HAp formation, but lower cytocompatibility at higher concentrations than their hybrid-source-derived counterparts.

4.1 $43SiO_2$-$25Na_2O$-$7P_2O_5$-(25-x) CaO-(x)MgO (x = 0, 5, 10, and 15 wt%)

4.1.1 Compositional analysis of as-quenched glasses

EDS analysis was used to determine the elemental composition of the as-quenched glasses. The measured compositions were consistent with the nominal compositions of the glasses. **Table ??** presents the elemental compositions (wt%) determined by EDS, with associated standard deviations (n=8). A representative EDS spectrum for the SC-0 glass is shown in **Fig.??**.

In addition to the nominal composition, trace elements, including MgO at levels below $\sim$ 1 wt%, were also detected as shown in (**Fig. ??** and **Table ??**). Notably, MgO was also observed even in the SC-0 glass, which lacked MgO addition in the nominal composition. Furthermore, Al_2O_3 was also detected with the level below $\sim$ 1 wt%. The presence of these trace elements is attributed to impurities in the starting materials of bio-wastes, as has been widely reported for agro-food waste ash [**? ?**].

4.1.2 Physical parameters

The density (ρ) of as-quenched glasses was calculated using Archimedes' method. These data were then used to deduce the molar volume (V_m), oxygen packing density (OPD), and oxygen molar volume (V_o) as shown in **Fig. ??**.

The density decreases with increasing MgO substitution for CaO. This observation is consistent with the lower molar mass of MgO (40.3 g/mol) compared to CaO (56.1 g/mol). The molar volume (V_m), representing the volume occupied by one mole of glass, also decreases with increasing MgO concentration. While density and molar volume typically exhibit an inverse relationship, the observed decrease in both parameters in these glasses can be attributed to the higher field strength and smaller ionic radius of Mg^{2+} (0.72 Å) compared to Ca^{2+} (1.00 Å) [**? ?**]. The higher field strength of Mg^{2+} leads to a more compact glass network due to stronger coulombic interactions with oxygen anions, resulting in an overall volume contraction despite the lower mass of MgO [**? ?**]. In other words, the impact of the increased field strength outweighs the effect of the lower molar mass, resulting in a net decrease in molar volume. Furthermore, to shed light on this anomalous behavior, the oxygen packing density was calculated, revealing a trend opposite to that of the molar volume (V_m). The increased compactness induced by MgO can be further explained by its higher polarizing power compared to CaO. The smaller ionic radius of Mg^{2+} results in a higher charge-to-size ratio, leading to stronger polarization of non-bridging oxygen (NBO) atoms and a more compact glass structure [**?**]. This effect reinforces the observed trends in density and molar volume. The deviation from linearity observed in these parameters with increasing MgO content is attributable to the mixed modifier effect, which typically arises when the ratio of the two modifiers approaches unity, influenced by their respective field strengths and electronegativities [**? ? ?**].

4.1.3 XRD analysis

The X-ray diffraction (XRD) patterns of all the as-quenched glasses are shown in **Fig.??**. The presence of a broad halo, instead of sharp peaks, confirms

the amorphous nature of the present glasses, indicating the absence of long-range translational order. In addition to a wide halo at a maximum of around 32°, another halo is also present at ∼ 20°. This secondary halo becomes more prominent with the addition of MgO in place of CaO.

This secondary halo suggests the possibility of phase separation within the glass matrix [**?**]. Several factors could contribute to this phenomenon. The higher field strength of Mg^{2+} compared to Ca^{2+} can promote immiscibility and phase separation [**?**]. The formation of P-O-Mg bonds, due to the disruption of the orthophosphate environment of P_2O_5 by MgO (as discussed in Section 4.1.4), may also contribute to phase separation. Furthermore, the presence of two glass formers, P_2O_5 and SiO_2, is known to generally lead to phase separation in glasses [**?** **?**]. The increasing tendency of the secondary halo with increase in MgO content indicates the increased phase separation tendency of the glasses. This observation is further supported by the presence of two glass transition temperatures (T_g) and two crystallization temperatures (T_c) determined from differential thermal analysis (DTA), as discussed in section 4.1.5.

4.1.4 Differential Thermal Analysis (DTA)

Differential thermal analysis (DTA) was performed to determine the glass transition temperature (T_g) and crystallization temperature (T_c) to assess thermal stability (Figure **??**). The thermographs reveal two T_g values: a subtle one between 300–400 °C (T_{g1}) and a more prominent one between 400–550 °$C(T_{g2})$. The derivative of the DTA curve (**Fig. ??**) confirms the presence of these two endothermic T_g peaks in all glasses. Both T_g values decrease with increasing magnesium content. T_{g1} is likely associated with the phosphate network, which typically exhibits a T_g in the 300–400 °C range [**?** **?**]. T_{g2} is attributed to the silicate glass network, usually observed between 450–600 °C [**?** **?**].

Despite the decreasing T_{g2} trend, the substitution of Ca^{2+} with Mg^{2+} leads to an increase in T_{c1} and a broadening of the crystallization peak, resulting in a wider sintering temperature window ($\Delta T = T_{c1} - T_{g2}$). This broadened

window is advantageous for processing, as it allows for sintering without unwanted crystallization. The enhanced stability and wider sintering window are attributed to the inhibitory effect of MgO on crystallization.

4.1.5 FTIR analysis

FTIR spectra of all the glasses show more or less similar spectra, with minor band splitting and shifting of the bands is observed with increasing MgO substitution (as shown in **Fig. ??)** To better understand the structural roles of SiO_2 and P_2O_5, FTIR spectra of all the glasses were deconvoluted **(Fig. ??)**. Deconvolution reveals bands from 500 to 1200 cm^{-1}, representing various structural units of both the glass networks.

In the silicate network, the Q^n notation (where n represents the number of bridging oxygens per silicon tetrahedron) is used to describe the structural units. The band at 840–846 cm^{-1} is attributed to Si-O stretching vibrations in Q^0 units. The band at ∼906–907 cm^{-1}, assigned to Q^1 units, remains relatively unchanged with MgO content, suggesting that Q^2 units dominate the present glass structure. The increase in peak area and FWHM of the bands at ∼1084–1098 cm^{-1} (Q^3 units) with increasing MgO substitution indicates an increase in the proportion of Q^3 structural units (as shown in the **Table ??**). This shift in Q^n distribution is reflected in the increasing ratios of $\frac{Q^3}{Q^2}$, $\frac{Q^3+Q^2}{Q^1}$, and $\frac{Q^3}{Q^2+Q^1}$ with increasing magnesium substitution. However, the ratio $\frac{Q^2}{Q^1}$ deviates from the linear trend, initially decreasing for SCM-5, then increasing for SCM-10, and finally slightly decreasing for SCM-15. Overall, these changes in structural units reveal increasing polymerization of the glass network. The band at 732 cm^{-1} is assigned to Si-O-Si stretching vibrations [**?** **?**].

Regarding the phosphate network, the band at 1034–1065 cm^{-1} represents vibrations of PO_4^{3-} tetrahedra with four non-bridging oxygen (NBO) atoms. The shoulder band at ∼586 cm^{-1} shifts to slightly lower wavenumbers with increasing MgO substitution, indicating asymmetric bending vibrations of the P-O bond and increased disorder in the orthophosphate environment[**?** **?**]. This increased disorder is potentially due to the formation of P-O-Mg bonds, facilitated by the higher electronegativity of Mg^{2+} (1.31) compared to Ca^{2+} (1.00) and Na^+ (0.93) [**?**]. The presence of orthophosphate units may also contribute to the observed phase separation in the glasses [**?** **?**].

Magnesium, with its higher field strength based on Dietzel's criteria, exhibits a dual nature, acting as both a network modifier and a former depending on its concentration [?]. Watts [?] reported that, in similar glass compositions (49.46 SiO_2 - 26.38 Na_2O - (23.8-x) CaO - 1.07 P_2O_5 - xMgO, where x ranges from 0 to 23.08 mol%), approximately 86% of the magnesium acts as a network modifier, while the remaining ∼14% acts as a network former. This dual behavior is reflected in the observed shifts in the SiO_2 and P_2O_5 bands: MgO addition causes the SiO_2-related bands to shift to higher wavenumbers (indicative of a network-forming role), while the P_2O_5-related bands shift to lower wavenumbers (indicative of a network-modifying role). This dual role of MgO further contributes to the increased phase-separation tendency. In essence, MgO promotes the formation of orthophosphate groups, which enhances phase separation in the glasses while simultaneously increasing the polymerization of the silicate network.

Further, a carbonate band is observed at ∼1482 cm^{-1} in all glass samples, which can be attributed to carbonate impurities present in the eggshell powder [? ? ?]. This band becomes more prominent upon the formation of carbonated hydroxyapatite (c-HAp), as discussed further in Section 4.4.2.

4.1.6 Thermal expansion coefficient (TEC)

TEC is related to the asymmetry of the interatomic potential well. As shown in **Table ??**, the TEC decreased with increasing MgO content, which can be attributed to the smaller ionic radius and higher field strength of Mg^{2+} compared to Ca^{2+} [?]. **Fig. ??** presents the dilatometric curves for the as-quenched glasses. A slight increase in TEC is observed for SCM-10, with a slight decrease in softening temperature (T_s) as compared to SCM-15 glass. This anomaly could be due to a mixed modifier effect as the MgO/CaO ratio approaches unity, resulting in increased competition between the two modifier oxides, which can lead to deviations in expected property trends [?].

The results observed for decreasing T_s are also consistent with DTA results with increasing MgO (**Table ??**), consistent with the DTA results. The ap-

proximately 30 °C difference between T_g and T_s is due to the different heating rates (i.e., 5 °C for TEC and 15 °C for DTA) employed in the two different techniques. The measured TEC values are within the range suitable for bioactive glasses, dentin, enamel coatings, and orthopedic substrates [**?**]. Importantly, the TEC of bioactive glasses can be adjusted through compositional modifications, allowing it to be tailored for specific applications like dental and orthopedic coatings while maintaining bioactivity [**?** **?**]. The TEC of SCM-15 is close to that of dentin and enamel ($8 \times 10^{-6} - 10 \times 10^{-6}$/°C) [**?**], suggesting its potential suitability for such applications.

4.1.7 Hardness

Hardness, a complex property influenced by bond strength, porosity, degree of polymerization, and fictive temperature. For oxide glasses, hardness is typically reported to be within the range of ∼2–8 GPa [**?**]. In the present study, Vickers hardness values ranged from 4.6 to 6.2 GPa (**Fig.??**).

Although MgO substitution for CaO is generally expected to increase hardness due to the higher field strength of Mg^{2+} (0.45 $Å^{-2}$) compared to Ca^{2+} (0.33 $Å^{-2}$), resulting in stronger bonds, a clear monotonic trend was not observed. Hardness initially increased from SC-0 (0 wt% MgO) to SCM-5 (5 wt% MgO), then decreased for SCM-10 (10 wt% MgO), and finally increased again for SCM-15 (15 wt% MgO). This non-linear behavior may be attributed to the mixed modifier effect, which is expected to be most prominent in SCM-10. SCM-5 exhibited the highest hardness among the series, potentially indicating increased network connectivity, which might be related to its lower bioactivity compared to other samples as discussed in the following sections. Initially, MgO may act as a network former, integrating into the SiO_2 network. However, with increasing MgO content, it may preferentially modify phosphate units, disrupting the glass network and leading to the observed non-linearity. The measured hardness values align with the reported hardness of 45S5 glass (4.58 ± 0.094 GPa) and other heat-treated bioglass/bioceramic systems [**?** **?**].

4.1.8 *In-vitro* testing of glasses

4.1.8.1 Biodegradability and pH change in SBF

The bioactive properties and degradation behavior of the glasses were evaluated by immersing them in simulated body fluid (SBF) for various durations at constant temperature. **Fig.??** shows the weight change (**Fig. ??(a)**) and pH variation (**Fig. ??(b)**) of the glasses over time. SC-0 exhibited the greatest weight loss, while SCM-15 showed the least.

SC-0 and SCM-5 showed the most rapid weight loss within the first two days of immersion. SC-0 then showed a weight gain at 5 days, followed by weight loss at 10 days, finally stabilizing at 20 days. SCM-5, after its initial weight loss, exhibited continuous weight gain up to 20 days. Glasses with higher MgO concentrations (SCM-10 and SCM-15) showed slower dissolution during the first two days, with maximum weight loss observed at 5 days, followed by continuous weight gain up to 20 days. The increasing MgO content correlates with slower degradation. This is likely because SC-0 contains only CaO (which is more hydrophilic than MgO), while the other glasses contain a mixture of CaO and MgO in different ratios. The distinct behavior of SC-0 can be attributed to the presence of only one alkaline earth metal oxide (CaO) in its composition. Moreover, CaO is more hydrophilic in nature in comparison to MgO [**?**].

Interestingly, SCM-15 showed minimal weight change. This might be attributed to the mixed-modifier effect of the MgO/CaO combination, where a ratio approaching unity hinders dissolution due to the competitive interaction of the two modifier ions [**?**]. Similar weight change trends have been reported for other bioactive glasses derived from agro-food waste and mesoporous bioactive glass [**?** **?**].

Further, the pH variation provides insights into the dissolution process. The pH change is directly related to the physicochemical reactions and ion exchange between the glass and the SBF. All glasses exhibited degradation, and the pH variation was non-uniform over time. The initial pH rise is attributed to the

release of base ions (Ca^{2+}, Na^+, and Mg^{2+}) and their interaction with H^+ and H_3O^+ ions, followed by the release of acidic Si^{4+} ions at later stages [? ?]. This process eventually reaches equilibrium, resulting in a stabilized pH. The release of base ions can be represented as follow:

$$\text{Si-O-Ca}^{2+} + \text{H}^+ \rightarrow \text{Si-OH}^- + \text{Ca}^{2+} \tag{4.1}$$

This pH increase leads to the formation of silicic acid ($Si(OH)_4$) near the glass surface, which in turn stabilizes the pH and facilitates attack on the silica network by SBF. MgO-substituted glasses showed a non-uniform pH trend at 5 days. However, after 10 days, glasses with higher magnesium content (SCM-10 and SCM-15) exhibited smaller pH changes than SC-0 and SCM-5, potentially due to slower Si^{4+} release. This observation is supported by MP-AES results (section 4.1.8.3), indicating lower silicate concentrations in SBF for SCM-10 and SCM-15. These results suggest that magnesium substitution increases chemical durability and hinders Si^{4+} release, consistent with the weight change results.

A further pH increase suggests reabsorption of Ca^{2+} and PO_4^{3-} ions from the SBF to form hydroxyapatite (HAp) on the glass surface. This pH increase slows as the solution becomes saturated, and the ion exchange rate decreases. Calcium phosphate (Ca-P) ions from the glass and SBF form a Ca-P-rich layer, which gradually incorporates carbonate ions (CO_3^{2-}) from the SBF, forming carbonated HAp (c-HAp) [?]. Slower dissolution and pH variation lead to more stable HAp formation. The c-HAp formation is driven by ion exchange and influences the dissolution rate, which can be optimized by adjusting modifier type and concentration. Using a single modifier like CaO promotes faster HAp growth, while incorporating two modifiers (e.g., CaO and MgO) moderates the dissolution rate, beneficial for applications requiring slow degradation [? ?]. The pH variation was recorded up to 40 days, at which point dissolution was observed for all glasses.

4.1.8.2 MP-AES analysis

Microwave plasma-atomic emission spectrometry (MP-AES) was employed to quantify ion concentrations in SBF after immersing the glasses for 20 days. **Table ??** shows the concentrations of Si^{4+}, Ca^{2+}, Mg^{2+}, and Na^{+} in SBF, along with changes in Ca and P content (wt%) in the glasses before and after immersion, as determined by EDS analysis. The Ca/P molar ratio calculated from EDS data is also included.

SC-0 exhibited the highest ion release, possibly due to a less polymerized glass network. The release of alkali ions and their exchange with H^{+} ions are crucial for bone bonding and regeneration [**? ?**]. The uneven release of sodium is recorded for all the glasses. However, increasing amounts of magnesium retards the liberation of sodium. This may be attributed to the dual role of MgO and the incorporation of Na^{+} ions into $(MgO_4)^{2-}$ tetrahedral for charge balancing [**?**].

The release of silica was highest for SC-0, with increasing magnesium having minimal impact on Si^{4+} release. This ion must be released from the interconnected glass network in the form of the Si-OH^{-} group. Silicon ion release from the glass network may occur later in the apatite formation process, as the glass network weakens after immersion in SBF, and the increase in magnesium in the glass sample replacing CaO results in a decrease in the amount of leached Ca^{2+} ion in the solution. Interestingly, the decrease in Ca^{2+} ions in the solution indicates increased Ca^{2+} in the glasses, as shown in the EDS result of the immersed samples (discussed in the section below 4.1.9), which suggests the deposition of Ca^{2+} from the solution to the glasses. This trend is in accordance with the saturation of the pH value and the increase in the weight of the samples, as explained in the section above.

4.1.9 FE-SEM with EDS analysis

The FE-SEM micrographs (Fig.8) show an appreciable surface modification of the glasses after the immersion of glass samples with increasing time in SBF

solution. A heterogeneous hydroxyapatite (HAp) layer develops on all glasses after 20 days of immersion in SBF (as shown in **Fig. ??**). SC-0 and SCM-15 show progressive HAp layer growth, while SCM-5 exhibits slower development even after 20 days, this may be due to the higher network connectivity in the SCM-5 glass as discussed earlier. FE-SEM images show a heterogeneous, spongy layer that forms on the SC-0 surface, along with small flakes. For SCM-5 and SCM-15, small, heterogeneously distributed clusters of white aggregates are observed. SCM-15 shows a more pronounced formation of the HAp layer compared to SCM-5 and SCM-10. EDS analysis of these white aggregates is presented in **Table ??**.

The Ca/P molar ratio for SC-0, SCM-5, and SCM-10 (ranging from 2.8 to 4.1) was higher than the standard stoichiometric ratio for hydroxyapatite (HAp) (1.67). However, the Ca/P ratio for SCM-15 (1.63) was close to the standard stoichiometric value, suggesting enhanced bioactivity for this composition. While a Ca/P ratio of 1.67 is often considered ideal for HAp, values between 2.8 and 4.1 have also been reported for carbonated HAp (c-HAp) in bioactive glasses [? ? ?]. This higher Ca/P ratio can be attributed to heterogeneity in the c-HAp layer caused by trace elements present in the starting materials, particularly when agro-food wastes were used as the sustainable resources to synthesize the glasses [?]

The distribution of various elements in SCM-15 without immersion and after immersion for 20 days is confirmed using area mapping, as shown in **(Fig.4.1)** , which confirms the elemental distribution. It is evident from these figures that a HAp rich layer is formed on the immersed SCM-15 glass.

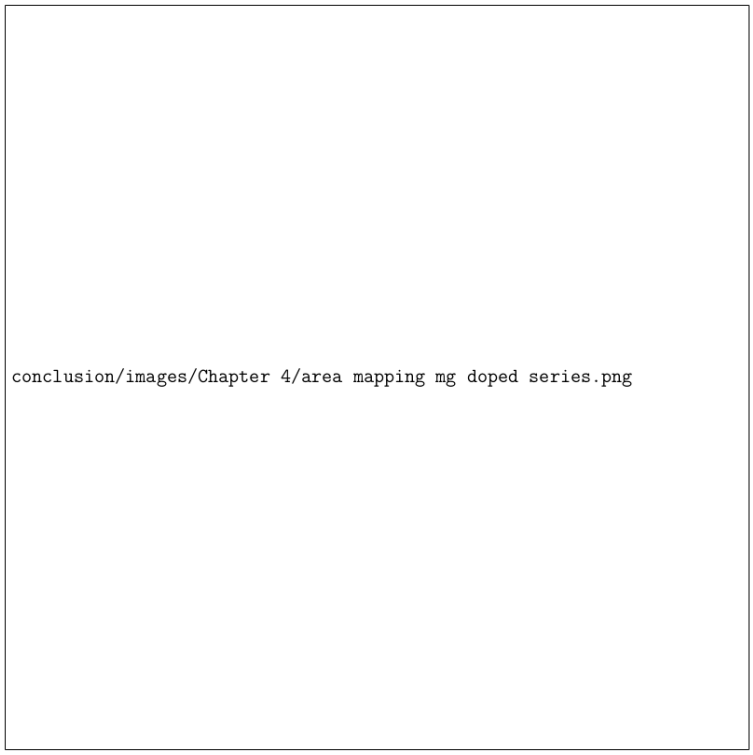

Figure 4.1: EDS area mapping of SCM-15 glass: (a) before immersion and (b) after immersion for 20 days

4.1.10 XRD analysis after immersion

XRD patterns of the glass samples before and after immersion in SBF are shown in **Fig. ??**. Minimal changes are observed in immersed glasses as compared to the pristine glasses. After immersion, weak diffraction peaks corresponding to semi-carbonated hydroxyapatite (HAp) (ICDD card no. 01-072-1243) appear in all immersed samples. In SC-0, a few feeble peaks indexed with tetracalcium phosphate (TTCP) (ICDD card no. 01-070-1379) are also present. The main constituents of tetra calcium phosphate are calcium (Ca) and phosphorus (P),

the primary elements found in the structure of the bone matrix. The phase primarily occurs as an intermediate between the HAp layer's formation with the Ca/P ratio >2, and can be beneficial for cell adhesion and bone regeneration [? ?].

In the magnesium-substituted glasses, HAp formation is not detected by XRD within the first 5 days of immersion. This suggests that Mg^{2+} initially retards HAp formation but may ultimately enhance its stability. The slower degradation of these glasses indicates increased glass network interconnectivity due to magnesium. However, prolonged immersion leads to the breakage of bonds formed by magnesium, followed by the formation of a silanol layer and subsequent development of the HAp layer. As the XRD pattern of all the glasses shows no formation of the HAp layer, the data for 2 days is omitted for further studies.

4.1.11 FTIR analysis after immersion in SBF

FTIR spectra of the glass samples after immersion in SBF for various durations are shown in **Fig. ??**. Deconvoluted was done to **(Fig.??)** analyze the changes in the bands compared to the pristine glasses. While the deconvoluted spectra reveal variations in the trends among the different glass compositions, the most significant changes are observed after 20 days of immersion, except for SCM-15. The band at ~910 cm^{-1} gradually merges with a sharper band at ~1015 cm^{-1} (attributed to phosphate units), with the latter's intensity increasing with immersion time.

In the fingerprint region, SCM-10 and SCM-15 exhibit similar behavior. Deconvolution reveals increased intensity and a shift towards higher frequencies compared to the pristine glasses, consistent with the expected changes upon SBF immersion. These changes highlight the interplay between silanol and phosphorus units in forming the hydroxyapatite (HAp) layer. Specifically, the shoulder band at 580 cm^{-1} increases in intensity, and the appearance of phosphate and carbonate bands, along with band splitting, further confirms the formation of carbonated HAp (c-HAp) [**?** **?**].

After immersion, the phosphate and carbonate bands observed on the glass surface resemble those of synthetic c-HAp and HAp formed on mineral-based bioactive glasses [**?**]. It is contradictory that magnesium with 15% substitution forms a better c-HAp layer than SCM-5 and SCM-10 glasses; this might be due to the relatively weaker bond strength of Mg-O-Si bonds compared to Si-O-Si bonds, which could facilitate glass degradation with increasing immersion time [**?**]. These results are in trend with magnesium at 5 wt% and afterward, opposite in the trend compared to the earlier reports in the literature for higher magnesium substitution [**?** **?**]. This contrasting behavior may be related to the association of higher MgO content with the phosphate glass network, as discussed in Section 4.1.4. However, it is well documented in the literature that magnesium enhances the bioactive properties by promoting cell proliferation and osteointegration [**?**].

4.1.12 MTT assay

The MTT assay was performed to evaluate the effect of the glasses on the viability of peripheral blood mononuclear cells (PBMCs) at concentrations up to 200 μg/ml **(Fig.??)(a)**. Cell viability was also monitored over 48 hours using a constant concentration of 100 μg/ml **(Fig.??)(b)**. The results indicate that cell viability remained above 85% for all glasses up to 200 μg/ml and after 48 h of treatment with 100 μg/ml.

According to ISO 10993-5, a substance is considered cytotoxic if it reduces cell viability by more than 30% [**?** **?**]. None of the tested glasses exhibited cytotoxicity to PBMCs, even at the highest concentration (200 μg/ml) or after 48 h of exposure (100 μg/ml). This finding was confirmed by a one-way ANOVA test ($p < 0.05$). Notably, glasses like SC-0 and SCM-10, which showed poorer HAp layer formation in previous studies, did not exhibit any cytotoxic effects. Interestingly, SCM-5 resulted in the highest cell proliferation among the glasses. The cytocompatibility of MgO-doped bioactive glass, showing no toxic effects at 100 μg/ml on normal human fibroblast cells, has been previously reported [**?**]. The glasses tested in the present study demonstrate excellent cytocompatibility with PBMCs.

4.2 43SiO_2-25CaO-7P_2O_5(25-y)Na_2O-(y)K_2O (y = 0, 5, 10, and 15 wt%)

Similar to the MgO-substituted series, these glasses were synthesized via the melt-quench technique. This series systematically replaces Na_2O with K_2O. The as-prepared glasses and those immersed in simulated body fluid (SBF) were characterized using various techniques, with the results and discussion presented in the following subsections.

4.2.1 Compositional Analysis

Energy-dispersive X-ray spectroscopy (EDS) was employed to analyze the composition of the melt-quenched glasses. The measured compositions of the pristine glasses closely matched the nominal compositions, with trace amounts of additional elements also detected. As with the MgO-substituted series, SC-0 serves as the control glass. Similar to the previous series, trace amounts of MgO and Al_2O_3 (below 1 wt%) were detected

4.2.2 Physical parameters

The density (ρ) of the glasses was measured using Archimedes' method as discussed earlier and given in ection 3.3.1. As shown in **Fig. ??**, increasing K_2O substitution for Na_2O results in a decrease in density (from 2.70 g/cm^3 to 2.61 g/cm^3) and a corresponding increase in molar volume. This inverse relationship between density and molar volume is expected. The observed trend is attributed to the substitution of the smaller Na^+ (1.02 Å) with the larger K^+ (1.34 Å), indicating that ionic size has a more significant effect than the atomic mass of Na_2O and K_2O. The larger K^+ ions disrupt the glass network, creating a more open structure and increasing the molar volume. This is consistent with the decreasing oxygen packing density and increasing oxygen molar volume observed with increasing K_2O [**? ? ?**]. The lower field strength of K^+ (0.52 $Å^{-2}$) compared to Na^+ (0.96$Å^{-2}$) [**?**] further contributes to the more open, less compact glass structure. This increased openness might lead to higher

dissolution rates in SBF, as discussed in section 4.2.8.

4.2.3 XRD analysis

XRD patterns of the glasses are presented in **Fig. ??**. A broad hump between 25° and 37°, indicates the amorphous structure of the present glasses. This characteristic hump arises from the presence of short-range order and the absence of long-range order. A secondary halo is also present at ∼20° in SC-0 glass only.

With increasing K_2O substitution for Na_2O, the main hump become broad, while the secondary halo diminishes and eventually disappears at 15 wt% K_2O (SNK-15). This suggests a decrease in immiscibility and a corresponding increase in homogeneity with K_2O content. This trend is attributed to the replacement of the higher field strength Na^+ (0.96 $Å^{-2}$) with the lower field strength K^+ (0.52$Å^{-2}$) [**?**], as higher field strength cations generally promote immiscibility [**?**]. Furthermore, the main hump shifts slightly to lower angles with increasing K_2O, consistent with increased homogeneity and the larger ionic radius of K^+ compared to Na^+.

4.2.4 Differential thermal analysis

DTA was used to determine the glass transition temperature (T_g), and crystallization temperature (T_c) to evaluate the thermal stability of the glasses. DTA curves are shown in **Fig.??**, and the derived thermal properties are summarized in

Both T_g and T_c exhibit an increasing trend with increasing K_2O content, consistent with the findings of Avramov et al. [**?** **?**]. This trend is attributed to the spatial hindrance effect of the larger K^+ ion compared to Na^+ . The larger K^+ hinders the mobility of modified SiO_4^{4-} tetrahedra, reducing devitrification and increasing T_g and T_c [**?**]. The conversion of some NBOs to BOs, as observed in the FTIR spectra section 4.3.5, is likely to contribute to this increase.

The onset of T_c increases with higher K_2O, and the T_c peaks broaden. This broadening suggests slower crystallization, potentially due to the disruption of the glass network by the larger K^+ ions and the mixed alkali effect, where the presence of both Na^+ and K^+ creates competing interactions that hinder crystallization [**?**]. Overall, there is an increase in thermal stability ($\Delta T = T_c - T_g$) with increasing K_2O, reaching 160 °C for SNK-15. This wider sintering window (ΔT) can be advantageous for biomedical applications requiring high sintering temperatures and delayed crystallization [**?**].

4.2.5 FTIR analysis

FTIR spectra of the glasses (**Fig. ??**) reveal slight band shifts and broadening, indicative of changes in the silicate and phosphate networks with increasing K_2O content in the glasses. Higher K_2O concentrations influence the silicate structural units, causing bands, particularly in the 800-1200 cm^{-1} range associated with Si-O-Si and P-O bond vibrations, to shift to lower wavenumbers and broaden [**?**]. This broadening suggests an increase in structural disorder, likely due to the larger size of K^+ (1.34 Å) compared to Na^+ (0.96 Å) [**?**].

Initially, adding K_2O disrupts the silicate network, decreasing the intensity of the 1012 cm^{-1} band and forming Si-OH^- groups at 1226 cm^{-1}, which enhances water absorption and benefits the physiochemical reactions during in vitro testing [**?**]. Increasing K_2O up to 10 wt% causes slight shifts in the 500-700 cm^{-1} range and intensifies the 1012 cm^{-1} band without silanol group formation as compared to SNK-5 and SNK-15 glass. Above 10 wt% K_2O, this band's intensity decreases, with the emergence of a silanol band, indicating a stronger mixed alkali modifier effect (Na_2O/K_2O ratio ∼1). Mixed modifier effects are known to be most prominent when the ratio of two modifier oxides, mixed former, and mixed intermediate oxides approaches unity, as discussed earlier and widely reported in the literature [**? ?**].

To further investigate the structural changes, the fingerprint region was deconvoluted as shown in **Fig. ??**. Bands in the 500-730 cm^{-1} range are attributed to Si-O-Si stretching, while the band at 587 cm^{-1} corresponds to

P-O bending vibrations [**?**]. These bands are relatively weak due to the low phosphorus content. In the 740-1200 cm^{-1} range, the intense band around ~909 cm^{-1} denotes NBO-O-Si asymmetric stretching, with the dominance of Q^1 units increasing with K_2O [**?**]. The band at 1031-1065 cm^{-1} represents changes in PO_4^{3-} vibrations, and the band at 1480 cm^{-1} is attributed to carbonyl groups, potentially related to carbonate remained in the eggshell pores [**?**], which is also observed in the MgO-series glasses (as discussed in the section 4.2.5).

FTIR analysis reveals an increase in the proportion of Q^1 and Q^3 structural units with increasing K_2O content, coupled with a decrease in Q^2 units. This trend suggests a conversion of some NBOs to BOs, as shown in the deconvoluted spectra (**Table ??**). To further quantify these changes, the fractions (f_0, f_1, f_2, f_3) of the different Q^n units were calculated using the following equations:

$$f_0 = \frac{A(Q^0)}{A(Q^0) + A(Q^1) + A(Q^2) + A(Q^3)} \tag{4.2}$$

$$f_1 = \frac{A(Q^1)}{A(Q^0) + A(Q^1) + A(Q^2) + A(Q^3)} \tag{4.3}$$

$$f_2 = \frac{A(Q^2)}{A(Q^0) + A(Q^1) + A(Q^2) + A(Q^3)} \tag{4.4}$$

$$f_3 = \frac{A(Q^3)}{A(Q^0) + A(Q^1) + A(Q^2) + A(Q^3)} \tag{4.5}$$

where $A(Q^n)$ represents the area of the corresponding Q^n peak.

The calculated f_n values, presented in **Table ??**, show that f_0 and f_2 decrease with increasing K_2O, while f_1 and f_3 increase. Overall, the results indicate an increase in the odd structural units as compared to the even structural units. This trend is likely due to the mixed alkali effect arising from the presence of both Na^+ and K^+ modifiers [**?**].

4.2.6 Thermal expansion coefficient

The thermal expansion coefficient (TEC) exhibits a non-linear trend with increasing K_2O substitution. The TEC initially increases from SC-0 to SNK-5, then decreases for SNK-10 and SNK-15 (**Table ??**). The highest TEC ($17 \times 10^{-6}/°C$) is observed for SNK-5, and the lowest ($10 \times 10^{-6}/°C$) for SNK-10. SNK-15 shows a slight increase in TEC ($12 \times 10^{-6}/°C$). While a decreasing TEC generally suggests the formation of stronger bonds, the non-linearity in this series complicates this interpretation. The softening temperature (T_s) increases with increasing K_2O, consistent with the DTA results and indicative of enhanced thermal stability. The measured TEC values fall within the range reported for bioactive glasses, human teeth, coatings for orthopedic substrates, and enamel ($8–10 \times 10^{-6}/°C$) [**?** **?**].

4.2.7 Hardness of pristine glasses

The Vickers hardness of the pristine glasses, as shown in **Fig. ??**, increases with increasing K_2O content, ranging from ∼4.6 to 6.02 GPa. However, SNK-10 deviates from this trend, potentially due to the more pronounced mixed-modifier effect discussed in the above sections. Despite K^+ having a lower field strength than Na^+, substituting Na^+ with K^+ does not decrease the hardness. This may be attributed to local structural distortions introduced by the K^+ substitution, potentially increasing hardness [**?**]. These values fall within the acceptable range for bioactive glasses [**?**], surpassing even Hench's glass. The increase in BOs relative to NBOs with increasing K_2O, along with decreased phase separation, may contribute to the enhanced hardness. The absence of fractures during indentation (**Fig. ??**) indicates good fracture toughness of these glasses. In other words, the developed glasses may have better technological properties like machinability etc.

The K_2O series exhibited lower hardness values (5.3–6.02 GPa) compared to the MgO series (6.2–6.5 GPa). This difference may be attributed to the more open glass structure resulting from the larger size of K^+ replacing Na^+ compared to the smaller Mg^{2+} replacing Ca^{2+}. This open structure is also consistent with the lower thermal stability observed in the K_2O series compared to the MgO series. However, both series exhibit higher thermal stability and hardness compared to the SC-0 control glass (4.6 GPa). The mixed modifier effect, evident in both series as the ratio of modifiers approaches unity, likely contributes to the non-linear trends observed in various properties.

4.2.8 *In-vitro* testing of bioactivity

4.2.8.1 Biodegradability

The pH change of the SBF solution upon glass immersion (**Fig. ??(a)**) is a key indicator of bioactivity. Initially, a rapid pH increase from 7.34 to 8.2 within 10 days is observed, driven by the release of Na^+, K^+, and Ca^{2+} ions from the glasses into the SBF and their exchange with H^+ or H_3O^+ ions. The change in

the pH value is related to the dissolution of the glasses in SBF. As discussed in FTIR analysis (section 4.3.5), the formation of the Si-OH^- group increases with K_2O content. So, it is responsible for early changes in pH values and the degradability of glasses.

This elevated pH indicates the dissolution of the silica glass network, resulting in the formation of better silanol groups and a subsequent decrease in pH in the second step. The fluctuations in pH over time are governed by the overall concentration of acidic ions like Si^{4+} and basic ions such as K^+, Ca^{2+}, and Na^+ in the SBF. After the initial surge, there is typically marginal or no further change in pH, indicating a stabilization of the ion exchange process between SBF and glasses [1–4]. Chemically, it can be explained as follows:

$$\text{Si-O-}K^+/Na^+ + H^+ \rightarrow \text{Si-}OH^- + K^+/Na^+ \tag{4.6}$$

The pH and weight changes of the glasses during immersion in SBF (**Fig. ??**) are closely related and reflect alterations in the chemistry of the glass surface due to ion leaching from the glasses. This pH decrease suggests potential network breakage due to leaching of the glassy matrix, exposing a fresh surface and reducing the demand for H^+ ions. SNK-5 and SNK-15 show higher biodegradability, likely facilitated by Si-OH^- groups (section 4.2.3), which promote HAp layer formation. Conversely, SNK-10's continuous pH increase is attributed to ongoing Si^{4+} leaching, supported by MP-AES analysis. SNK-10 also shows less Ca^{2+} and Na^+ leaching, consistent with its weight gain at 20 days. Among the K_2O glasses, SNK-5 exhibits the greatest weight loss, and SNK-15 the least, with SNK-15 reaching maximum weight gain at 20 days. This weight gain correlates with reduced Ca^{2+} in SBF and its deposition on the glass surface (EDS analysis, **Table ??(b)**). K_2O glasses show continuous weight gain up to 40 days, unlike SC-0, which shows weight loss after 20 days. As discussed previously, the single alkali oxide glass (SC-0) shows a different weight loss trend, likely due to its higher initial Ca^{2+} leaching and resulting porosity in the immersed glasses. This difference influences the kinetics of HAp

formation and dissolution. The pH and weight changes after SBF immersion are related to HAp layer formation. Furthermore, the presence of two modifiers in comparable ratios can significantly alter the glass behavior. Therefore, glass compositions can be tailored for specific needs and applications in the human body.

4.2.9 MP-AES analysis

MP-AES was used to quantify ion concentrations in SBF after glass immersion for 20 and 40 days (**Table ??**). The results indicate that among the glass containing K_2O, increasing K_2O concentration results in the maximum leaching across all the glasses, indicating heightened susceptibility to physicochemical reactions compared to reference SC-0 glass. As previously discussed, the formation of Si-OH^- groups increases with increasing K_2O concentration. The lower field strength of K^+ compared to Na^+ might be the possible reason behind increased leaching. The physiochemical reactions between alkali ions and H^+ ions play an important role in bone bonding and regeneration.

Compared to the reference (control) glass SC-0, all K_2O-containing glasses exhibit higher Si^{4+} ion leaching, which is directly associated with glass dissolution. This indicates that glass degradation initiates upon immersion in SBF through the reaction between silica tetrahedral units and water. SNK-15, however, demonstrates less Si^{4+} leaching than SNK-5 after both 20 and 40 days, consistent with the observed decrease in pH after 20 days and the reduced weight loss for this glass observed after 20 days.

Furthermore, K_2O enhances the release of modifier ions (Ca^{2+} and Na^+) while reducing Si^{4+} release. IReplacing Na^+ with K^+ appears to facilitate modifier ion leaching while hindering Si^{4+} leaching. Similar trends for Ca^{2+} and Na^+ release with increasing K_2O in S53P4 glass have been reported by Massera et al. [**?**]. This enhanced modifier ion release may contribute to the improved HAp layer formation observed on the SNK-5 and SNK-15 glass surfaces. In contrast, SNK-10 shows the opposite trend, releasing more Si^{4+} than modifier ions. This higher Si^{4+} release delays the formation of the silanol

layer and subsequently the calcium phosphate layer, as evidenced by the XRD analysis of SNK-10. This may explain the less pronounced HAp layer formation on SNK-10, even after extended immersion for 20 and 40 days, which is also supported by FE-SEM-EDS analysis.

This series exhibits increased glass dissolution compared to the MgO series. The addition of MgO retards Si^{4+} ion release, likely contributing to the slower and delayed HAp layer formation compared to the K_2O series. In the K_2O series, the higher dissolution of calcium and Si^{4+} ions, compared to both the control glass and the MgO series, promotes earlier formation of the silanol layer, which subsequently facilitates HAp layer development.

4.2.10 FE-SEM and EDS analysis of *in-vitro* tested glass

Fig. ?? shows the morphological changes in the glasses before and after immersion in SBF. Initially, a sponge-like layer forms on the glass surface, followed by the development of spherulite or globular structures composed of flakes. These structures grow over the spongy layer with increasing immersion time, particularly evident in SNK-5 and SNK-15 over 20 and 40 days. The increasing calcium (Ca) and phosphorus (P) content observed in EDS analysis confirms the development of an HAp layer on the glass surface after immersion.

Interestingly, all glasses with K_2O addition exhibit better HAp layer formation than the glasses without K_2O and glasses with MgO addition (as explained in first series). However, SNK-10 (10 wt% K_2O) shows less prominent HAp growth than SNK-5 and SNK-15 even after 40 days. This could be due to continuous Si^{4+} leaching into SBF, delaying the formation of the Si-OH^- layer necessary for calcium phosphate deposition. This observation is consistent with the XRD, FTIR, and MP-AES results.

EDS mapping reveals a carbonated hydroxyapatite (c-HAp) layer on all glasses, supported by the increased intensity of the CO_3^{2-} band in FTIR spectra. The Ca/P ratios for the K_2O glasses (3.4–2.26) are higher than the standard stoichiometric HAp ratio (1.67). Notably, SNK-15 shows a significant decrease

in Ca/P ratio, approaching the values reported for c-HAp in the literature [?]. The formation of the HAp layer in the present glasses contrasts with results reported in the literature for the glasses synthesized using conventional chemicals with K_2O substitution, where K_2O is reported to retard the HAp layer formation on the glasses [? ? ?].

4.2.11 XRD analysis after immersion of glasses in SBF

XRD patterns of the pristine glasses and after immersion in SBF for various durations are shown in **Fig. ??**. Minor changes are observed after immersion, with weak diffraction peaks corresponding to semi-crystalline hydroxyapatite (HAp) (ICDD card no. 01-072-1243) appearing at $2\theta \approx 32^\circ$ in all immersed glasses. Feeble peaks corresponding to tetracalcium phosphate (TTCP) (ICDD card no. 01-070-1379) are also observed. TTCP, composed primarily of calcium and phosphorus, often appears as an intermediate phase during HAp formation, particularly when the Ca/P ratio is > 2 [? ?].

No HAp formation is detected in SNK-5, SNK-10, and SC-0 glass after 2 days of immersion in SBF. In contrast, SNK-15 shows weak peaks for both HAp and TTCP after 2 days, with stable HAp formation up to 40 days. Both, SNK-5 and SC-0 show both phases after 5 days. The stable HAp formation is recorded in SNK-5 and SNK-15 samples compared to SC-0 glass. No HAp is observed in SNK-10 after 5 days; however, weak TTCP peaks appear after 10 days, and HAp forms after 40 days. This delayed HAp formation in SNK-10 is consistent with the weight change and MP-AES analysis of SBF.

Similar to the MgO series, minimal changes are observed in the K_2O glasses after 2 days of immersion. However, HAp layer formation occurs earlier in the K_2O series compared to the MgO series. The TTCP phase is observed in all K_2O glasses, likely due to the consistent calcium content, unlike the MgO series where CaO is systematically replaced. Similar to SCM-10, SNK-10 exhibits delayed formation of both TTCP and HAp, possibly due to the mixed modifier effect. The comparable concentrations of Na_2O and K_2O in SNK-10 and CaO and MgO in SCM-10 likely lead to a competitive interaction between

these modifiers, influencing the observed behavior.

4.2.12 FTIR analysis after *in-vitro* testing

FTIR spectra of the glasses after immersion in SBF reveal notable changes in their structural composition as shown in **Fig.??**. The increased full width at half maximum (FWHM) with immersion time indicates greater structural disorder and porosity. The intense Si-OH^- band at ∼1200 cm^{-1} appears in all glasses at different immersion times [**?**]. The band at ∼910 cm^{-1} gradually merges with the phosphate band at ∼1025 cm^{-1} as the immersion time increases.

SNK-5 and SNK-15 show intense phosphate bands after 20 days, while SNK-10 exhibits delayed dissolution, with a strong phosphate band appearing only after 40 days. The early formation of the silanol layer (after 5 days) in SNK-5 and SNK-15 suggests that it acts as a precursor to HAp formation. In the fingerprint region, all samples show similar behavior, with increasing intensity of the P-O bending band at ∼587 cm^{-1} and the appearance of a new band at 605 cm^{-1}, indicating HAp formation [**?** **?**]. The pronounced band at ∼1450 cm^{-1} (CO_3^{2-}) confirms the formation of carbonated hydroxyapatite (c-HAp), consistent with EDS results. SNK-10 shows significant changes in the Si-O-Si stretching band at 910 cm^{-1} [**?**], in correlation with the extensive Si^{4+} leaching observed in MP-AES analysis, likely contributing to its delay in HAp formation.

Deconvoluted FTIR spectra (**Fig. ??**) provide more detailed insights into structural changes. The deconvoluted spectra show increased intensity and shifts to higher frequencies compared to pristine glasses, which is expected after SBF immersion. These findings underscore the exciting transformations in glass's structural composition with immersion time, highlighting the interplay between silanol and phosphorus units in forming HAp layers. The distinct behavior of the SNK-10 samples, with its delayed yet intense changes, offers intriguing insights into the dissolution and reformation processes in bioactive glasses. Interestingly, carefully selecting two distinct modifiers in an approxi-

mate ratio of 1 may help to develop bioactive materials with improved thermal and corrosion resistance. These materials can be tailored to have either higher or lower pH values, making them suitable for compatibility with human plasma as well as fillers in teeth.

FTIR results indicate more pronounced structural changes in the K_2O series compared to the MgO series. The K_2O glasses exhibit intensified silanol bands, even in the pristine state, potentially due to their more open structure. This open structure, compared to the MgO series, likely leads to greater structural modification upon immersion. The FTIR spectra also reveal more intense c-HAp formation in the K_2O series compared to both the MgO series and the control glass.

4.2.13 MTT assay

The MTT assay was used to evaluate the effect of the glasses on cell viability at concentrations up to 200 μg/ml as shown in **Fig.??(a)**. Additionally, the effect on human peripheral blood mononuclear cells (PBMC) was monitored over different time durations up to 48 h using a constant concentration of 100 μg/ml (**Fig.??(b)**). The results demonstrated that cell viability remained unaffected across all glasses at concentrations up to 200 μg/ml and even after 48 h of treatment with 100 μg/ml.

The findings of the present bioglasses reveal that none of the glasses were cytotoxic to PBMC, maintaining viability above the threshold value i.e., >30% according to ISO10993-5 standard as mentioned earlier [**?**] . Statistical analysis using a one-way ANOVA test confirmed no significant differences among the treated cells ($p < 0.05$). Interestingly, glasses with less HAp formation (SC-0 and SNK-10) did not show cytotoxic effects. Notably, SC-0 exhibited high cell proliferation. The biocompatibility of K_2O-doped mesoporous bioactive glass has been previously reported at a concentration of 20 μg/ml on human normal fibroblast cells [**?**]. Overall, the present glasses demonstrate excellent cytocompatibility with PBMCs.

In contrast to the MgO series, the K_2O glasses exhibit lower cell viability over time. The MgO series maintains high viability (up to 85% at 200 µg/ml and 94% at 100 µg/ml) even after 48 hours. While the K_2O glasses initially show comparable viability (up to 86% at 200 µg/ml), viability decreases over time, reaching 83% for SNK-5 and 85% for the other K_2O glasses. This reduced viability in the K_2O series may be attributed to the higher ion leaching rate compared to the MgO series (Section 4.3.9).

4.3 Comparative study of glasses

Based on bioactivity, biocompatibility, and other properties of glasses, three of the best compositions were also synthesized using only conventional to validate and compare the results with glass synthesized by hybrid sources i.e., biowaste and conventional chemicals. Glasses with composition $43SiO_2$-$25CaO$-$25Na_2O$-$7P_2O_5$, $43SiO_2$-$10CaO$-$15MgO$-$25Na_2O$-$7P_2O_5$, and $43SiO_2$-$10CaO$-$10Na_2O$- $15K_2O$-$7P_2O_5$ are designated as MS-0, MM-15, and MK-15, respectively. The properties of these synthesized glasses are discussed below and compared with those of the hybrid-source-derived glasses of similar compositions.

4.3.1 Physical paramters

The densities of the conventionally prepared glasses MS-0, MM-15, and MK-15 are 2.8 g/cm^3, 2.64 g/cm^3, and 2.7 g/cm^3, respectively. These values are slightly different from the hybrid-source-derived glasses i.e., SC-0, SCM-15, and SNK-15 glass. However, the trends in density and molar volume remain consistent across both sets of glasses. **Table ??** summarizes the density, molar volume (V_m), and oxygen packing density (OPD) of the conventional glasses compared with those derived from hybrid-sources.

Similar to the hybrid-source-derived series, the addition of MgO in MM-15 leads to a decrease in both density and molar volume compared to MS-0. This is attributed to the smaller ionic radius and higher field strength of Mg^{2+} relative to Ca^{2+}, resulting in a more compact network [**? ?**]. Conventionally derived glasses exhibit slightly higher density and OPD and lower V_m compared to their hybrid counterparts. This difference is likely due to the higher porosity often observed in bioactive glasses derived from biowaste sources [**? ?**].

Likewise, MK-15 exhibits a decrease in density and an increase in molar volume is observed compared to MS-0, which is consistent with the potassium-substituted hybrid-source-derived glasses. This is due to the substitution of the smaller Na^+ ion (1.02 Å) with the larger K^+ ion (1.34 Å), which disrupts the network, resulting in a more open structure and an increased molar volume.

This structural change is also reflected in the lower oxygen packing density. The lower field strength of K^+ (0.52 $Å^{-2}$) compared to Na^+ (0.96 $Å^{-2}$) further contributes to this less compact structure [? ? ?]. These results confirm that hybrid-source-derived glasses exhibit a more open structure compared to conventionally derived glasses.

4.3.2 XRD analysis

XRD analysis confirmed the amorphous nature of all conventionally prepared glasses, as evidenced by the broad halo observed around 32° (**Fig. ??**). Similar to the hybrid series, a second halo at ∼20° is present in MS-0. This second halo becomes more prominent with MgO addition in MM-15 in comparison to MS-0 glass, mirroring the trend observed in the hybrid sources obtained MgO glasses and suggesting an increased tendency for phase separation. As discussed previously, network-modifying cations with higher field strengths can promote phase separation [?].

In contrast, the 20° halo disappears entirely with K_2O addition (MK-15), indicating decreased phase separation, consistent with the observations in the hybrid-source-derived K_2O glasses i.e., SNK-15. This is likely due to the substitution of the higher field strength Na^+ (0.96 $Å^{-2}$) with the lower field strength K^+ (0.52 $Å^{-2}$) [?]. Higher field strength cations are known to increase immiscibility. The slight shift of the main hump to lower angles with increasing K_2O content further supports increased homogeneity and is consistent with the larger ionic radius of K^+ compared to Na^+. Thus the XRD pattern of hybrid sources derived glasses and conventional chemical derived glasses are more or less follow the similar trend.

4.3.3 Differential thermal analysis (DTA)

DTA was performed on the conventionally prepared glasses (as shown in **Fig. ??**)to determine their thermal properties and compare them with the hybrid-source-derived glasses. The results, summarized in **Table ??**, show similar trends to the hybrid-source-derived glasses. As expected, T_g decreases with

MgO addition (MM-15) and increases with K_2O addition (MK-15).

The decrease in T_g for MM-15 compared to MS-0 can be attributed to the dual nature of MgO and the formation of $(MgO_4)^{2-}$ tetrahedra, which can disrupt the silicate network and lead to weaker Si-O-Mg bonds compared to Si-O-Si bonds. This observation aligns with trends in other MgO-containing bioglasses [**?**]. The presence of Na^+ ions might also contribute to this T_g decrease due to ion mixing or preferential bonding [**?**]. Similar to the hybrid-source-derived glasses, the presence of two T_c values, especially in MM-15, suggests an increased tendency for phase separation. Broadening of the crystallization peaks with increasing MgO is also observed, consistent with the XRD results (Section 4.4.2).

In MK-15, the increase in T_g compared to MS-0 aligns with the behavior of the K_2O-containing hybrid-source-derived glasses and can be attributed to the spatial hindrance effect of the larger K^+ ion compared to Na^+, as discussed previously in section 4.3.4. This effect restricts the mobility of modified SiO_4^{4-} tetrahedra, reducing devitrification [**?**]. The broadening of the T_c peak in MK-15 suggests slower crystallization, potentially due to glass network disruption by the larger K^+ ions and the mixed alkali effect [**?**]. Overall, the addition of K_2O leads to increased thermal stability ($\Delta T = T_c - T_g$), beneficial for biomedical applications requiring high sintering temperatures and delayed crystallization [**?**]. The thermal behavior of the conventionally derived glasses closely resembles that of the hybrid-source-derived glasses, validating the use of biowaste for synthesizing bioactive glasses with high thermal stability.

4.3.4 FTIR analysis

The FTIR spectra of the conventionally derived glasses (as shown in **Fig.??** show similar bands to their hybrid-source-derived glasses, primarily featuring silicate-related bands in the 800-1200 cm^{-1} region.

As observed in the hybrid sources derived series with SCM-15, the MM-15 sample exhibits a slight shift of these bands to higher wavenumbers compared

to MS-0. The bands between ∼851 and ∼1200 cm^{-1} are attributed to Si-O-Si asymmetric stretching, with possible overlap from phosphorus-related bands in the 900-1200 cm^{-1} region [? ?]. The shoulder band at ∼1014 cm^{-1} shows a slight decrease in intensity with MgO addition. Similar to SCM-15, minor changes are observed in the bands at ∼916 cm^{-1} and ∼850 cm^{-1}. The band at ∼706 cm^{-1}, present in all samples, corresponds to Si-O-Si symmetric stretching vibrations [?]. Additionally, the band at ∼565 cm^{-1} is assigned to P-O asymmetric bending vibrations. [?].

In MK-15 glass, a slight broadening of the spectra is observed, particularly in the 800-1200 cm^{-1} region. This broadening suggests an increase in structural disorder, likely due to the larger cationic size of K^+ (1.38 Å) compared to Na^+ (1.02 Å) [?]. Similar bands to those observed in MS-0 and MM-15 are also present in MK-15, indicating the presence of both silicate and phosphate structural units. However, the intensity of the ∼916 cm^{-1} band increases with K_2O addition (MK-15), consistent with the trend observed in the K_2O-substituted hybrid-source-derived glasses.

To further investigate these structural changes, the different Q^n structural units and their fractions (f_n) were quantified using deconvoluted FTIR spectra in the 600-1200 cm^{-1} region. The results follow a similar trend to that observed in the hybrid-source-derived glasses. With increasing MgO concentration, Q^3 and Q^2 units increase relative to Q^1 units. K_2O addition, on the other hand, leads to an increase in the odd-numbered structural units (Q^3 and Q^1) relative to Q^2, as shown in **Table ??**. Overall, the FTIR spectra of the conventionally derived glasses are largely consistent with those of the hybrid-source-derived series.

4.3.5 Thermal expansion coefficient

The TECs of the conventionally prepared glasses (MS-0, MM-15, and MK-15) are approximately similar but marginally higher than those of the hybrid-source-derived glasses. MS-0 has a TEC of 15.1 × 10^{-6}/°C. Both MM-15 and MK-15 exhibit lower TEC values, 14 × 10^{-6}/°C and 15 × 10^{-6}/°C, respectively.

The softening temperatures (T_s), summarized in **Table ??**, are also comparable to those of the hybrid-derived glasses and consistent with the T_g values obtained from DTA. This similarity in thermal properties between the conventional and hybrid glasses suggests comparable behavior in terms of thermal response of both type of glasses synthesized using two different sources.

The measured TEC values are within the range suitable for various biomedical applications, including bioactive glasses, dentin and enamel coatings, and orthopedic substrates [**? ?**].

4.3.6 Hardness

The microhardness of the glasses MS-0, MM-15 and MK-15 is 6.6, 6.25, and 6.3 GPa, respectively, These values are higher compared to their hybrid counterparts: SC-0 (4.8 GPa), SCM-15 (6.1 GPa), and SNK-15 (6.02 GPa).This difference might be due to the formation of more covalent bonds in the conventionally prepared glass structure, leading to increased rigidity and compactness. These results are also consistent with the density and FTIR results of MS-0, MM-15, and MK-15 glasses. This suggests that conventionally derived glasses have greater rigidity than those derived using hybrid sources. However, the hardness of these conventional glasses is still within the range reported for bioactive glasses [**?** **?**]. However, these glasses shows cracks in comparison to those of hybrid glasses, indicating that these have low fracture toughness as compared to the hybrid glasses as shown in Fig.

4.3.7 *In-vitro* testing

The *in-vitro* bioactivity of the conventionally prepared glasses (MS-0, MM-15, MK-15) was evaluated and compared with that of their hybrid sources derived glasses (SC-0, SCM-15, SNK-15).

4.3.7.1 Biodegradability test

The weight change and pH variation during immersion in SBF provide insight into the biodegradability of glasses. **Fig. ??** shows the results for the conventional glasses.

MS-0 and MM-15 exhibited maximum weight losses of 5.9% and 6.6%, respectively, after just two days of immersion in SBF. Unlike the gradual weight loss observed for the hybrid-derived glass SC-0, MS-0 showed a more rapid initial weight loss, potentially due to the higher reactivity of conventional chemicals. This higher reactivity is also reflected in the earlier formation of HAp observed in the XRD analysis of MS-0 (section 4.3.10). Following the initial weight loss, MS-0 showed a weight gain throughout the immersion period, ex-

cept for a slight weight fluctuations after 20 days of immersion. This fluctuation could be due to the formation of an intermediate phase formation, as observed in the XRD analysis. The weight change trend of MS-0 is consistent with its pH change profile as shown in **Fig. ?? (a)**.

MM-15 showed a similar initial weight loss to its hybrid source derived glass, SCM-15. However, MM-15 exhibited higher weight gain after 5 days, possibly due to the increased reactivity of the conventional chemicals. Similar to SCM-15, the addition of MgO in MM-15 slow down the degradation rate, resulting in only marginal weight changes throughout the immersion period. This slower degradation correlates with the slower release of Si^{4+} observed in the MP-AES results for MM-15. The pH changes in the SBF solutions are non-uniform and consistent with the observed weight changes, reflecting alterations in the glass surface chemistry due to ion leaching and HAp formation, as discussed in sections 4.2.8, and 4.3.8.

MK-15 exhibited a maximum weight loss of 5 wt% after 2 days, compared to 3.8 wt% for SNK-15 at the same time period. Like SNK-15, MK-15 showed a weight increase after 5 days, consistent with the formation of an intermediate phase observed in the XRD analysis. A slight weight loss at 10 days was followed by relatively stable weight until 20 days of immersion, after which a continuous weight increase was observed up to 40 days. This behavior is more or less same as the trend observed for SNK-15. Overall, both MS-0 and MM-15 show different weight change profiles after 40 days compared to SC-0 and SCM-15, respectively. This suggests differences in the long-term stability of the HAp layer formed on the conventionally derived glasses with respect to the hybrid-derived glasses.

4.3.8 MP-AES analysis

MP-AES analysis was performed to quantify ion concentrations in SBF after immersing the MS-0, MM-15, and MK-15 glasses for 20 and 40 days. **Table ??** shows the concentrations of Si^{4+}, Ca^{2+}, Mg^{2+}, Na^{+}, and K^{+} in SBF, along with changes in Ca and P content (wt%) in the glasses before and after immersion,

as determined by EDS analysis. The Ca/P molar ratios calculated from EDS data are also included.

MS-0 exhibited the highest Si^{4+} ion release compared to the other glasses, consistent with the trend observed in the hybrid-source-derived glasses. However, these conventionally prepared glasses showed less ion release in comparison to those of their hybrid source counterparts, possibly because of the more polymerized structure of the conventional glasses, as suggested by the density and FTIR analysis. Additionally, our earlier study revealed that eggshell-derived CaO exhibits a different conversion profile and higher porosity compared to conventional $CaCO_3$, potentially retaining some carbonate groups even at 1000 °C [**?**]. This difference in the CaO precursor may contribute to the higher ion leaching observed in the hybrid-source-derived glasses. Furthermore, the decrease in Si^{4+} release in the case of MM-15 glass indicates the slower Si^{4+} release, which may contribute to the more heterogeneous HAp layer formed on their surfaces, as shown in FESEM micrographs. Similarly, results have been observed in the case of magnesium-substituted SCM-5, SCM-5,10, and SCM-15 glasses reported in the present study. The slower ion release might be the possible reason behind the continuous pH increase even after 20 days in the MM-15 glass, corresponding to the delayed but continuous ion exchange reaction between SBF and glasses. Furthermore, the MM-15 sample shows less leaching of the Mg^{2+} as compared to the SCM-15 glass, which might be the possible reason behind the better formation of the HAp layer as compared to the SCM-15 glass indicating higher release of Mg^{2+} in SCM-15 glass, as magnesium is highly reported to decrease the crystallization tendency of HAp layer [**?**]. However, the sodium ion leaching is non-uniform in all the glasses and higher as compared to the hybrid-soruce derived glasses. The decrease in the leaching of Ca^{2+} in MS-0 and MM-15 glasses after 40 days is due to the formation of the HAp layer on the glass surface as observed in the EDS analysis.

In MK-15 glass, the lower Ca^{2+} release could be the reason for the less dense HAp layer formed compared to SNK-15 glass. However, MK-15 glass indicates the release of higher amounts of the Ca^{2+} and other ions, except

silica as compared to MS-0, and MM-15 glass, followed by a decrease in the Ca^{2+} in the solution after 40 days. Overall, the results indicate less Ca^{2+} and Si^{4+} ion release from the conventionally prepared glasses compared to the hybrid-source-derived glasses, which can be attributed to the high porosity of the agro-food waste-derived glasses, as reported previously [**?**].

4.3.9 FESEM-EDS analysis

FE-SEM analysis reveals appreciable changes on the glass surfaces after 20 and 40 days of SBF immersion (**Fig. ??**). After 20 days, all samples show non-uniform distribution of the HAp layer due to surface inhomogeneity. The HAp layer become homogeneous over time with increasing thickness of the layer. MS-0 and MM-15 exhibit small spherical crystals, more pronounced than those observed on SC-0 and SCM-15 glass. After 40 days, flaky structures appear on MS-0 and MM-15, indicating further layer growth. This enhanced HAp formation on the mineral-based glasses could be due to faster ion exchange compared to the hybrid-source-derived glasses, potentially due to the less Mg^{2+} leaching (compared to SCM-15 glass), which is known to retard c-HAp crystallization. However, the EDS analysis indicates a higher Ca/P ratio (as shown in **Table ??**) as compared to the SC-0 and SCM-15 glass samples (Ca/P ratios of 4.1 and 1.6, respectively) after 20 days. The Ca/P ratios for MS-0 and MM-15 glass were approximately 2.45 and 2.20 after 40 days, indicating more stable layer formation compared to SC-0 and SCM-15, which showed dissolution after 20 days.

For MK-15, FE-SEM micrographs reveal less spongy layer formation compared to SNK-15. This could be attributed to the reduced Ca^{2+} ion release from MK-15, as observed in the MP-AES analysis. The reduced spongy layer formation, followed by the development of a flaky structure after 40 days of immersion, suggests less homogeneous HAp formation on MK-15 compared to SNK-15. This observation is further supported by the higher Ca/P ratio for MK-15.

4.3.10 XRD analysis after *in-vitro* test

XRD patterns of the pristine and SBF-immersed glasses are shown in **Fig.??**. After immersion, all glasses exhibit weak diffraction peaks corresponding to semi-crystalline hydroxyapatite (HAp) (ICDD card no. 01-072-1243), superimposed on the amorphous hump, as formation of HAp is a surface phenomenon [**?**]. In contrast to the hybrid-source-derived glasses, HAp peaks appear in MS-0 and MM-15 after just two days of immersion and remain stable up to 40 days, indicating more rapid and stable HAp layer formation.

In MS-0, weak peaks corresponding to tetracalcium phosphate (TTCP) (ICDD card no. 01-070-1379) are observed at 20 and 40 days immersion in SBF, appearing later than in SC-0, where TTCP is present at all time points. This delayed TTCP formation in MS-0 might explain its higher Ca/P ratio after 20 and 40 days. MM-15, however, does not exhibit any peaks corresponding to the TTCP phase, likely due to its lower Ca^{2+} content, similar to the SCM-15 glass. Further, MK-15 shows fewer and weaker HAp peaks compared to SNK-15 glass, indicating delayed HAp formation than SNK-15 glass. This delay may be attributed to the reduced Ca^{2+} leaching observed in MPAES analysis in MK-15 glass compared to SNK-15 glass.

4.3.11 FTIR analysis after immersion

FTIR spectra of the glasses after varying SBF immersion times (**Fig. ??**) reveal changes in their structural composition. The increased FWHM observed for all glasses with increasing immersion time indicates an increased structural disorder. The intense Si-OH^{-} band at ∼1200 cm^{-1} is present in all glasses at different time intervals [**?**]. The prominent Si-O-Si stretching band at ∼910 cm^{-1} gradually merges with the phosphate band at ∼1025 cm^{-1} as immersion time increases [**? ?**].

MS-0 and MK-15 exhibit highly intense phosphate bands after 20 days of immersion, similar to SC-0 and SNK-15 samples, while MM-15 shows a slow and continuous increase in this band with increasing immersion time, followed by an intensified band corresponding to phosphate units after 40 days. The early formation of the silanol layer suggests it acts as a precursor to HAp formation. In the fingerprint region, all samples show similar behavior, with increased intensity of the P-O^{-} bending band at ∼587 cm^{-1} [**? ?**]. The band at 735 cm^{-1} gradually disappears with immersion time, suggesting increased disorder in the silicate structure. The pronounced CO_3^{2-} band at ∼1450 cm^{-1} confirms the formation of carbonated hydroxyapatite (c-HAp), consistent with the EDS results [**? ?**]. Overall, the FTIR spectra confirm c-HAp formation on all glass surfaces with increasing immersion time. The most significant changes are observed in MS-0 and MK-15, potentially due to higher silica leaching compared to MM-15, resulting in a more intense Ca-P layer.

4.3.12 MTT assay

Fig.?? shows the cell viability of the conventionally derived glasses (MS-0, MM-15, and MK-15) after 24 h of incubation with PBMCs at concentrations up to 200 μg/ml. In contrast to the hybrid-source-derived glasses, which maintained high viability even at 200 μg/ml, the conventional glasses exhibited a decrease in cell viability to ∼70% at just 50 μg/ml. This decrease might be attributed to the higher initial leaching of alkali ions (e.g., Na^{+}) from the conventional glasses, potentially causing a cytotoxic effect. High alkali ion release

and its negative impact on cell viability have been reported in the literature [? ? ?].

The faster ion release from the conventional glasses compared to the hybrid glasses could also contribute to this reduced cytocompatibility. Similar findings have been reported by Wallace et. al [?] and Tilocca [?], suggesting that a rapid release of alkali ions, rather than a balanced release of calcium (essential for cell viability and interfacial bonding), can be detrimental. Due to the significant decrease in viability observed at 50 μg/ml, a lower concentration (25 μg/ml) was used for the time-dependent cell viability test (up to 48 h). All conventional glasses, except MK-15, maintained acceptable cell viability up to 48 h. MK-15 showed a decrease to 64% viability after 48 h. Overall, the hybrid-source derived glasses exhibited higher cell viability (>80%) as compared to their conventionally derived glasses.

4.4 Summary

The MgO substitution for CaO increased the phase separation as compared to the control glasses. MgO exhibiting a dual role increased the polymerization within the silicate network, and act as modifier in the phosphate glass network. In contrast, K_2O substitution for Na_2O enhanced structural homogeneity and promoted the conversion of NBOs to BOs, increasing the proportion of odd-numbered Q^n units. Both MgO and K_2O widened the sintering window and increased hardness compared to the control glass, although a mixed modifier effect caused non-linear trends. *In vitro*, MgO glasses showed delayed c-HAp formation and less stable HAp formation (Ca/P = 1.63 after 20 days) but superior cytocompatibility. K_2O glasses exhibited faster and stable c-HAp formation (Ca/P = 2.2 after 40 days) but reduced cytocompatibility over time due to higher ion leaching. Conventionally derived glasses, compared to their hybrid counterparts, had higher density, faster and more stable HAp formation (Ca/P = 2.4–4.5 after 40 days), increased hardness, but lower fracture toughness and reduced cytocompatibility. Overall, the hybrid-source-derived glasses show better bioactive properties compared to the conventional precursor-derived glasses.

These results demonstrate the impact of modifier type and precursor source on bioactive glass properties and biological response, informing composition design for specific applications.

Chapter 5

Conclusion and future scope

Conclusion

Two glass series, $43SiO_2$-$25Na_2O$-$7P_2O_5$-(25-x)CaO-xMgO (x = 0, 5, 10, 15 wt%) and $43SiO_2$-25CaO-$7P_2O_5$-(25-y)Na_2O-yK_2O (y = 0, 5, 10, 15 wt%), were synthesized using hybrid sources i.e., biowaste-derived (SiO_2 and $CaCO_3$) and conventional chemical precursors via melt-quenching. These series were characterized to analyze the structural, thermal, and mechanical properties using various characterization techniques. Further, *in-vitro* bioactivity and biocompatibility assessments with human PBMCs were conducted. Bases on the results obtained, three of the best compositions were also synthesized using only conventional precursors for comparison. The conclusion of the present study is given below:

All the glasses were amorphous in nature with some phase separation tendency. With MgO substitution, the phase separation tendency increases, while K_2O substitution enhances homogeneity and decreases phase separation in the glasses. MgO plays the dual role by acting as an former and modifier in the silicate and phosphorus glass network. Overall, the addition of MgO increases the polymerization On the other hand, whereas K_2O promoted conversion of some fraction of NBOs to BOs, increasing odd-numbered Q^n units. Both modifiers enhances the thermal stability and widened the sintering window. The TECs were within the range suitable for bioactive glass applications in coatings

of enamel and other osteo- and orthopedic substrates. Both MgO and K_2O increased hardness as compared to control glasses. However, both series show mixed modifier effects, causing deviations from linearity in different properties of glasses as well as in the bioactive properties.

During *in-vitro* testing, all the glasses shown the formation of the c-HAp layer on the glasses. However, the formation of c-HAp depends upon the density of the glasses and substituted components. The best bioactivity and biocompatibility is observed in $43SiO_2$-$25CaO$-$25Na_2O$-$7P_2O_5$ (Sc-0) glass. MgO substitution retarded Si^{4+} release and delayed c-HAp formation. On the other hand, K_2O increased ion leaching, accelerating c-HAp formation. Both the glasses show cytocompatibility of $>85\%$ for up to $200\mu g/ml$, however, K_2O shows less cytocompatibility as compared to the MgO series glasses over the time test due to higher leaching of ions in the K_2O series. The SNK-15 glass with $43SiO_2$-$25CaO$-$7P_2O_5$-$(10)Na_2O$-$15K_2O$ shows the maximum bioactivity.

The conventionally derived glasses exhibited better physical, structural, and mechanical properties as compared to their hybrid-source-derived counterparts. However, the bioactive properties and cytocompatibility are higher in the hybrid-source-derived glasses. This approach of hybrid sources (biowaste + conventional chemicals) can be used to develop bioactive materials without hampering their other properties. This approach is cost-effective and sustainable in nature. In fact, it shows better results than conventional chemicals.

Future scope of the present work

Further research should investigate:

1. These synthesized glasses using a hybrid approach are promising candidates for body implants, bone tissue engineering, and dental applications. However, the present glasses require more extensive *in-vivo* testing, including cytotoxicity and therapeutic efficacy evaluations, to prove the safety profile for translational usage.
2. The specific influence of two alkali modifiers in the (MgO, K_2O)-containing glasses warrants detailed investigation, particularly for potential dental

filling applications. Further optimization of these compositions could lead to enhanced properties and performance.

3. This approach using biowaste-derived precursors offers a cost-effective and sustainable alternative to conventional synthesis, often yielding materials with competitive or even superior properties. Further research and development in this area could pave the way for innovative and environmentally friendly biomaterials.

Navneet_OPP

ORIGINALITY REPORT

14%	9%	11%	3%
SIMILARITY INDEX	INTERNET SOURCES	PUBLICATIONS	STUDENT PAPERS

PRIMARY SOURCES

1	www.researchgate.net Internet Source	1%
2	Submitted to Thapar University, Patiala Student Paper	1%
3	www.science.gov Internet Source	<1%
4	Shivani Punj, Kulvir Singh. "Bioactive calcium silicate glass synthesized from sustainable biomass wastes", Biofuels, Bioproducts and Biorefining, 2020 Publication	<1%
5	www.frontiersin.org Internet Source	<1%
6	tudr.thapar.edu:8080 Internet Source	<1%
7	www.mdpi.com Internet Source	<1%
8	www.intechopen.com Internet Source	<1%
9	Submitted to Higher Education Commission Pakistan Student Paper	<1%
10	Praveen Jha, K. Singh. "Effect of MgO on bioactivity, hardness, structural and optical properties of SiO2–K2O–CaO–MgO glasses", Ceramics International, 2016 Publication	<1%

11	Sarita Pradhan, N.D. Chakladar. "Tailoring the composition of quaternary phosphate glass system for suitability in implant application", Ceramics International, 2025 Publication	<1 %
12	Shivani Punj, K. Singh. "Blue-green light emitting inherent luminescent glasses synthesized from agro-food wastes", Journal of Materials Science: Materials in Electronics, 2019 Publication	<1 %
13	pubs.rsc.org Internet Source	<1 %
14	Shih-Ching Wu, Hsi-Kai Tsou, Hsueh-Chuan Hsu, Shih-Kuang Hsu, Shu-Ping Liou, Wen-Fu Ho. "A hydrothermal synthesis of eggshell and fruit waste extract to produce nanosized hydroxyapatite", Ceramics International, 2013 Publication	<1 %
15	worldwidescience.org Internet Source	<1 %
16	Sakthi Prasad, Anustup Chakraborty, Kaushik Biswas. "Chapter 8 Melt-Derived Bioactive Glasses: Approaches to Improve Thermal Stability and Antibacterial Property by Structure–Property Correlation", Springer Science and Business Media LLC, 2022 Publication	<1 %
17	Nawaz, Qaisar. "Multifunctional SiO2-CaO Based Mesoporous Bioactive Glasses with Therapeutic Ion and Biomolecule Releasing Capability", Friedrich-Alexander-Universitaet Erlangen-Nuernberg (Germany), 2024 Publication	<1 %

18	Petrica Vizureanu, Seiji Yamaguchi, Madalina Simona Baltatu, Gültekin Göller et al. "Functionalized Materials Applications in Biomedicine", CRC Press, 2025 Publication	<1 %
19	hdl.handle.net Internet Source	<1 %
20	Praveen Jha, Satwinder Singh Danewalia, Gaurav Sharma, K. Singh. "Antimicrobial and bioactive phosphate-free glass–ceramics for bone tissue engineering applications", Materials Science and Engineering: C, 2018 Publication	<1 %
21	Shivani Punj, Neha Srivastava, Manoj Baranwal, Kulvir Singh. "In-vitro Biological Evaluation of Diopside Bio-ceramic Synthesized From Sustainable Agro-food Waste Ashes", Silicon, 2021 Publication	<1 %
22	Muhammad Shoaib, Ali Bahadur, Shahid Iqbal, Murefah Mana AL-Anazy et al. "Magnesium doped mesoporous bioactive glass nanoparticles: A promising material for apatite formation and mitomycin c delivery to the MG-63 cancer cells", Journal of Alloys and Compounds, 2021 Publication	<1 %
23	Mohamed Saiful Firdaus Hussin, Hasan Zuhudi Abdullah, Maizlinda Izwana Idris, Mohd Arizam Abdul Wahap. "Extraction of natural hydroxyapatite for biomedical applications—A review", Heliyon, 2022 Publication	<1 %
24	Submitted to Imperial College of Science, Technology and Medicine Student Paper	<1 %

25	scholar.ufs.ac.za Internet Source	<1%
26	Vijayakumari Sugumaran, Elakkiya Krishnamoorthy, Annamalai Kamalakkannan, Riju Chandran Ramachandran, Balakumar Subramanian. "Unscrambling the Influence of Sodium Cation on the Structure, Bioactivity, and Erythrocyte Compatibility of 45S5 Bioactive Glass", ACS Applied Bio Materials, 2022 Publication	<1%
27	Burcu Karakuzu-Ikizler, Pınar Terzioğlu, Yeliz Basaran-Elalmis, Bilge Sema Tekerek, Sevil Yücel. "Role of magnesium and aluminum substitution on the structural properties and bioactivity of bioglasses synthesized from biogenic silica", Bioactive Materials, 2020 Publication	<1%
28	brieflands.com Internet Source	<1%
29	Shivani Punj, Jashandeep Singh, K. Singh. "Ceramic biomaterials: Properties, state of the art and future prospectives", Ceramics International, 2021 Publication	<1%
30	Seun Samuel Owoeye, Davies Oladayo Folorunso, Fatai Aramide, Believe Okotie. "Microwave energy assisted fabrication and characterization of 45S5 bioglass-ceramics using bio-wastes as alternative resources for biomedical applications", Ceramics International, 2024 Publication	<1%
31	Submitted to Iona College Student Paper	<1%

32	Submitted to Queen's University of Belfast Student Paper	<1 %
33	thesis.univ-biskra.dz Internet Source	<1 %
34	Zeimaran, Ehsan. "A Poly (Octanediol Citrate)/Gallium-Containing Bioglass Composite for Bone Tissue Regeneration", University of Malaya (Malaysia), 2023 Publication	<1 %
35	mdpi-res.com Internet Source	<1 %
36	M. A. Madshal, G. El-Damrawi, M. El Baiomy, Amal Behairy. "Calcium Silicate Glass Ceramics Containing Chromium Sulfate: Structural, Optical, and Shielding Properties", Arabian Journal for Science and Engineering, 2024 Publication	<1 %
37	Manmeet Kaur Chhina, Kulvir Singh. " Photoluminescence and structural properties of air-reduced rare-earth ( ) doped calcium silicates derived using biomass wastes ", Biofuels, Bioproducts and Biorefining, 2021 Publication	<1 %
38	Submitted to University of Macau Student Paper	<1 %
39	theses.ucalgary.ca Internet Source	<1 %
40	Azevedo, H.S.. "Incorporation of proteins and enzymes at different stages of the preparation of calcium phosphate coatings on a degradable substrate by a biomimetic methodology", Materials Science & Engineering C, 20050428	<1 %

Publication

41	Boris Ildusovich Kharisov, Oxana Vasilievna Kharissova, Ubaldo Ortiz-Mendez. "CRC Concise Encyclopedia of Nanotechnology", CRC Press, 2019 Publication	<1 %
42	Jonathan Massera, Leena Hupa. "Influence of SrO substitution for CaO on the properties of bioactive glass S53P4", Journal of Materials Science: Materials in Medicine, 2013 Publication	<1 %
43	Manmeet Kaur Chhina, Navneet Kaur Mattu, K. Singh. "Dy doped calcium silicates synthesized using agro-food wastes and conventional chemicals as resources: A comparative study", Hybrid Advances, 2024 Publication	<1 %
44	Ryan West, Dérick Rousseau. "The role of nonfat ingredients on confectionery fat crystallization", Critical Reviews in Food Science and Nutrition, 2017 Publication	<1 %
45	cancer-nano.biomedcentral.com Internet Source	<1 %
46	www.ijser.org Internet Source	<1 %
47	Rongbin Dang, Na Li, Yuqiang Yang, Kang Wu, Qingyuan Li, Yu Lin Lee, Xiangfeng Liu, Zhongbo Hu, Xiaoling Xiao. "Designing advanced P3-type K0.45Ni0.1Co0.1Mn0.8O2 and improving electrochemical performance via Al/Mg doping as a new cathode Material for potassium-ion batteries", Journal of Power Sources, 2020 Publication	<1 %

48	www2.mdpi.com Internet Source	<1%
49	Gaurav Sharma, Manmeet Kaur, Shivani Punj, Kulvir Singh. "Biomass as a sustainable resource for value-added modern materials: a review", Biofuels, Bioproducts and Biorefining, 2020 Publication	<1%
50	Jibanjyoti Panda, Awdhesh Kumar Mishra, Yugal Kishore Mohanta, Kaustuvmani Patowary, Pradipta Ranjan Rauta, Bishwambhar Mishra. "Exploring Biopolymer for Food and Pharmaceuticals Application in the Circular Bioeconomy: An Agro-Food Waste-to-Wealth Approach", Waste and Biomass Valorization, 2024 Publication	<1%
51	Satwinder Singh, K. Singh. "Nanocrystalline glass ceramics: Structural, physical and optical properties", Journal of Molecular Structure, 2015 Publication	<1%
52	Submitted to Turun yliopisto Student Paper	<1%
53	res.mdpi.com Internet Source	<1%
54	Gaurav Sharma, K. Singh. "Recycling and utilization of agro-food waste ashes: syntheses of the glasses for wide-band gap semiconductor applications", Journal of Material Cycles and Waste Management, 2019 Publication	<1%
55	M. Mohan Babu, P. Venkateswara Rao, Nibu Putenpurayil Govindan, Raghavendra Gujjala, P. Syam Prasad. "Chapter 4 Structural and In	<1%

	Vitro Bioactivity of Phosphate-Based Glasses for Bone Regeneration", Springer Science and Business Media LLC, 2023 Publication	
56	Submitted to The Scientific & Technological Research Council of Turkey (TUBITAK) Student Paper	<1 %
57	Submitted to University of KwaZulu-Natal Student Paper	<1 %
58	c.coek.info Internet Source	<1 %
59	Saeid Kargozar, Sara Hooshmand, Seyede Atefe Hosseini, Sara Gorgani, Farzad Kermani, Francesco Baino. "Antioxidant Effects of Bioactive Glasses (BGs) and Their Significance in Tissue Engineering Strategies", Molecules, 2022 Publication	<1 %
60	Submitted to Universiti Sains Malaysia Student Paper	<1 %
61	Submitted to University of Aberdeen Student Paper	<1 %
62	umu.diva-portal.org Internet Source	<1 %
63	vdoc.pub Internet Source	<1 %
64	journals.sagepub.com Internet Source	<1 %
65	www.physics.uwo.ca Internet Source	<1 %
66	Hashmi, M.U., and Saqlain A. Shah. "Dissolution behavior of bioactive glass ceramics with different CaO/MgO ratios in	<1 %

SBF-K9 and r-SBF", Progress in Natural Science Materials International, 2014.
Publication

67	M. Anand Pandarinath, G. Upender, K. Narasimha Rao, D. Suresh Babu. "Thermal, optical and spectroscopic studies of boro-tellurite glass system containing ZnO", Journal of Non-Crystalline Solids, 2016 Publication	<1 %
68	M. Sarmast Sh, A. B. Dayang Radiah, D. A. Hoey, N. Abdullah, H. S. Zainuddin, S. Kamarudin. "The structural, mechanical, and biological variation of silica bioglasses obtained by different sintering temperatures", Journal of Sol-Gel Science and Technology, 2024 Publication	<1 %
69	Vargas Nadal, Guillem. "Novel Quatsome Nanovesicles, Prepared Using Compressed CO2, for the Development of Advanced Nanomedicines.", Universitat de Barcelona (Spain) Publication	<1 %
70	Zhi Wei Loh, Mohd Hafiz Mohd Zaid, Khamirul Amin Matori, Mohd Mustafa Awang Kechik et al. "Phase transformation and mechanical properties of new bioactive glass-ceramics derived from CaO–P2O5–Na2O–B2O3–SiO2 glass system", Journal of the Mechanical Behavior of Biomedical Materials, 2023 Publication	<1 %
71	repository.lib.ncsu.edu Internet Source	<1 %
72	123dok.net Internet Source	<1 %

73	Barbara Szpunar, Uwe Erb, Gino Palumbo, K. T. Aust, Laurent J. Lewis. "Magnetism in complex atomic structures: Grain boundaries in nickel", Physical Review B, 1996 Publication	<1 %
74	M. Vallet-Regí, A. Rámila, S. Padilla, B. Muñoz. "Bioactive glasses as accelerators of apatite bioactivity", Journal of Biomedical Materials Research Part A, 2003 Publication	<1 %
75	Murilo C. Crovace, Viviane O. Soares, Ana Candida M. Rodrigues, Oscar Peitl et al. "Understanding the mixed alkali effect on the sinterability and in vitro performance of bioactive glasses", Journal of the European Ceramic Society, 2021 Publication	<1 %
76	dos Santos Prezas, Pedro Rafael. "Polarização Elétrica de Biomateriais Baseados em Hidroxiapatite, como Filmes em Substratos Metálicos, para Aumento da Bioatividade", Universidade de Aveiro (Portugal), 2024 Publication	<1 %
77	s3-eu-west-1.amazonaws.com Internet Source	<1 %
78	Submitted to London Metropolitan University Student Paper	<1 %
79	M. El Baiomy, R.M. Ramadan, Y.M. Moustafa, G. El Damrawi. "Structural, optical, and radiation shielding parameters of zinc silicate glasses modified with erbium oxide", Optical Materials, 2024 Publication	<1 %
80	Submitted to University of Adelaide Student Paper	<1 %

81	Xavier Kesse, Charlotte Vichery, Jean-Marie Nedelec. "Deeper Insights into a Bioactive Glass Nanoparticle Synthesis Protocol To Control Its Morphology, Dispersibility, and Composition", ACS Omega, 2019 Publication	<1 %
82	arch.library.northwestern.edu Internet Source	<1 %
83	archive.org Internet Source	<1 %
84	Submitted to City University of Hong Kong Student Paper	<1 %
85	Fabian Zemke, Valerie Schölch, Maged F Bekheet, Franziska Schmidt. "Surfactant-assisted sol–gel synthesis of mesoporous bioactive glass microspheres", Nanomaterials and Energy, 2019 Publication	<1 %
86	Submitted to Jawaharlal Nehru Technological University Student Paper	<1 %
87	Lefebvre, L.. "Structural transformations of bioactive glass 45S5 with thermal treatments", Acta Materialia, 200706 Publication	<1 %
88	Submitted to Queen Mary and Westfield College Student Paper	<1 %
89	Submitted to University of Birmingham Student Paper	<1 %
90	Zhao, Mingming. "Quality Consistency Assessment for the Multi-Originated Chinese Herb Bupleuri Radix", University of Macau, 2023	<1 %

	Publication	
91	coewww.rutgers.edu Internet Source	<1%
92	www.hindawi.com Internet Source	<1%
93	James R. Bardill, Daewon Park, Ahmed I. Marwan. "Improved Coverage of Mouse Myelomeningocele With a Mussel Inspired Reverse Thermal Gel", Journal of Surgical Research, 2020 Publication	<1%
94	Tüncer, Melisa. "Green Synthesis of Nanostructured Bioactive Glass for Dental Applications.", Izmir Institute of Technology (Turkey) Publication	<1%
95	Submitted to University of Greenwich Student Paper	<1%
96	Submitted to University of Portsmouth Student Paper	<1%
97	biointerfaceresearch.com Internet Source	<1%
98	jesc.ac.cn Internet Source	<1%
99	www.outsourceaccelerator.com Internet Source	<1%
100	Submitted to Cranfield University Student Paper	<1%
101	Ding, J.. "The properties and structure of Sn@? Ca@?P@?O@?F glasses", Materials Chemistry & Physics, 20030928 Publication	<1%

102	M.H.G. Jacobs, H.A.J. Oonk. "Equilibrium Between Phases of Matter", Springer Science and Business Media LLC, 2012 Publication	<1 %
103	arxiv.iacs.res.in:8080 Internet Source	<1 %
104	coek.info Internet Source	<1 %
105	comptes-rendus.academie-sciences.fr Internet Source	<1 %
106	core.ac.uk Internet Source	<1 %
107	iopscience.iop.org Internet Source	<1 %
108	patents.google.com Internet Source	<1 %
109	www.rroij.com Internet Source	<1 %
110	B. Sasikumar, Santhosh J. Eapen. "Spices Production to Products - Purity and Authenticity", CRC Press, 2025 Publication	<1 %
111	Bose, S.. "Microwave-processed nanocrystalline hydroxyapatite: Simultaneous enhancement of mechanical and biological properties", Acta Biomaterialia, 201009 Publication	<1 %
112	Rayala, Tejeswar. "A Numerical Approach for Evaluating Fire Resistance of FRP-Strengthened Prestressed Concrete Beams.", Michigan State University Publication	<1 %

113	Rittermeier, André(Chemie). "Alternative catalysts for the synthesis of methanol in the liquid phase", Ruhr-Universität Bochum, Universitätsbibliothek, 2010. Publication	<1 %
114	Shanmukaraj, D.. "Characterization of PEG: LiClO"4+SrBi"4Ti"4O"1"5 nanocomposite polymer electrolytes for lithium secondary batteries", Journal of Power Sources, 20050926 Publication	<1 %
115	Submitted to University of the Assumption Pampanga Student Paper	<1 %
116	biblio.ugent.be Internet Source	<1 %
117	juser.fz-juelich.de Internet Source	<1 %
118	pubs.acs.org Internet Source	<1 %
119	pure.unileoben.ac.at Internet Source	<1 %
120	www.ncbi.nlm.nih.gov Internet Source	<1 %
121	www.tandfonline.com Internet Source	<1 %
122	Balogun, Olugbenga. "Anti-Inflammatory Effect of Onion Peel Extract in the Intestine.", North Carolina Agricultural and Technical State University Publication	<1 %
123	G. Rajkumar, S. Aravindan, V. Rajendran. "Structural analysis of zirconia-doped calcium	<1 %

phosphate glasses", Journal of Non-Crystalline Solids, 2010
Publication

124	Hasnat Zamin, Takeshi Yabutsuka, Shigeomi Takai, Hiroshi Sakaguchi, Takeshi Yao. "Fabrication of Bioactive Zirconia by Doubled Sandblasting Process and Incorporation of Apatite Nuclei", Key Engineering Materials, 2019 Publication	<1 %
125	Héctor Martínez Ávila, Eva-Maria Feldmann, Mieke M. Pleumeekers, Luc Nimeskern et al. "Novel bilayer bacterial nanocellulose scaffold supports neocartilage formation invitro and invivo", Biomaterials, 2015 Publication	<1 %
126	Kirill A. Afonin, Morgan Chandler. "Therapeutic RNA Nanotechnology - Immunomodulation and Dynamicity", Jenny Stanford Publishing Pte. Ltd., 2021 Publication	<1 %
127	M. Magallanes-Perdomo, A.H. De Aza, I. Sobrados, J. Sanz, P. Pena. "Structure and properties of bioactive eutectic glasses based on the Ca3(PO4)2–CaSiO3–CaMg(SiO3)2 system", Acta Biomaterialia, 2012 Publication	<1 %
128	Wynand JvdM Steyn. "Applications of Nanotechnology in Road Pavement Engineering", Nanotechnology in Civil Infrastructure, 2011 Publication	<1 %
129	biolres.biomedcentral.com Internet Source	<1 %
130	espace.library.uq.edu.au Internet Source	

		<1%
131	hb.diva-portal.org Internet Source	<1%
132	kaplaninterfaces.net.technion.ac.il Internet Source	<1%
133	kclpure.kcl.ac.uk Internet Source	<1%
134	pdffox.com Internet Source	<1%
135	piginny.com Internet Source	<1%
136	pure.kfupm.edu.sa Internet Source	<1%
137	Goel, A.. "The effect of Cr"2O"3 addition on crystallization and properties of La"2O"3-containing diopside glass-ceramics", Acta Materialia, 200808 Publication	<1%
138	Leenaporn Jongpaiboonkit, Travelle Franklin-Ford, William L. Murphy. "Growth of Hydroxyapatite Coatings on Biodegradable Polymer Microspheres", ACS Applied Materials & Interfaces, 2009 Publication	<1%
139	McEntire, B.J., B.S. Bal, M.N. Rahaman, J. Chevalier, and G. Pezzotti. "Ceramics and ceramic coatings in orthopaedics", Journal of the European Ceramic Society, 2015. Publication	<1%
140	Mozaniel Santana de Oliveira, Leo M.L. Nollet. "Bioactive Compounds - Identification and Characterization of their Food and Pharmacological Potential", CRC Press, 2025	<1%

Publication

141	R. Coziol. "The Relation between Galaxy Activity and the Dynamics of Compact Groups of Galaxies", The Astronomical Journal, 07/2004 Publication	<1 %
142	S. Rodino, N.L. Petculescu, V. Dragomir. "Capitalization of agro-food waste products within the sustainable bioeconomy", Acta Horticulturae, 2024 Publication	<1 %
143	Ting Zhu, Rui Chen, Aiping Li, Jia Liu, Dengan Gu, Qizhan Liu, Hebron C. Chang, Jianwei Zhou. "JWA as a Novel Molecule Involved in Oxidative Stress-Associated Signal Pathway in Myelogenous Leukemia Cells", Journal of Toxicology and Environmental Health, Part A, 2006 Publication	<1 %
144	Yuehua Dong, Yanjun Yang, Yulei Wei, Yongshan Gao, Weihua Jiang, Guigang Wang, Dawei Wang. "Facile synthetic nano-curcumin encapsulated Bio-fabricated nanoparticles induces ROS-mediated apoptosis and migration blocking of human lung cancer cells", Process Biochemistry, 2020 Publication	<1 %
145	Zainab M. Al-Rashidy, M.M. Farag, N.A. Abdel Ghany, A.M. Ibrahim, Wafa I. Abdel-Fattah. "Orthopaedic bioactive glass/chitosan composites coated 316L stainless steel by green electrophoretic co-deposition", Surface and Coatings Technology, 2018 Publication	<1 %
146	d.docksci.com Internet Source	<1 %

147	ebin.pub Internet Source	<1%
148	es.scribd.com Internet Source	<1%
149	krishikosh.egranth.ac.in Internet Source	<1%
150	m.moam.info Internet Source	<1%
151	qmro.qmul.ac.uk Internet Source	<1%
152	savoirs.usherbrooke.ca Internet Source	<1%
153	www.jkcs.or.kr Internet Source	<1%
154	www.oncotarget.com Internet Source	<1%
155	Cerruti, M.. "Effect of pH and ionic strength on the reactivity of Bioglass^(R) 45S5", Biomaterials, 200505 Publication	<1%
156	Liu, J.. "Oxygen reduction at sol-gel derived La"0"."8Sr"0"."2Co"0"."8Fe"0"."2O"3 cathodes", Solid State Ionics, 20060131 Publication	<1%
157	P. Bargavi, R. Riju Chandran, D. Durgalakshmi, P. Rajashree, R. Ramya, S. Balakumar. "Drug infused Al2O3-bioactive glass coatings toward the cure of orthopedic infection", Progress in Biomaterials, 2022 Publication	<1%
158	Rafael Borja, Ma José Fernández-Rodríguez. "Energy recovery as added value from food	<1%

and agricultural solid wastes", Elsevier BV, 2021
Publication

159	Shrikaant Kulkarni, Vipul Srivastava, Rabah Khenata, Yarub Al-Douri. "Advanced Materials for Next-Generation Technologies - ", Apple Academic Press, 2025 Publication	<1%
160	Carrasquillo Salib, Javier A.. "Microwave Assisted Synthesis of ZnO Nanoparticles, Copper/Indium-ZnO Nanocomposites and Photodegradability of Carbamazepine.", Universidad Ana G Méndez - Gurabo Publication	<1%
161	Gaurav Sharma, K. Singh. "Dielectric and optical properties of glasses and glass-ceramics synthesized from agro-food wastes", Materials Chemistry and Physics, 2020 Publication	<1%
162	V. Rajendran, M. Prabhu, R. Suriyaprabha. "Synthesis of TiO2-doped mesoporous nanobioactive glass particles and their cytocompatibility against osteoblast cell line", Journal of Materials Science, 2015 Publication	<1%

Exclude quotes	On	Exclude matches	Off
Exclude bibliography	On		